Metabolic Engineering 79 (2023) 159–172

Contents lists available at ScienceDirect

Metabolic Engineering

journal homepage: www.elsevier.com/locate/meteng

Time-resolved, deuterium-based fluxomics uncovers the hierarchy and dynamics of sugar processing by *Pseudomonas putida*

Daniel C. Volke [a,**], Nicolas Gurdo [a], Riccardo Milanesi [b], Pablo I. Nikel [a,*]

[a] The Novo Nordisk Foundation Center for Biosustainability, Technical University of Denmark, 2800, Kongens Lyngby, Denmark
[b] Department of Biotechnology and Biosciences, University of Milano-Bicocca, 20126, Milano, Italy

ARTICLE INFO

Keywords:
Pseudomonas putida
Metabolic flux analysis
Deuterium
Glycolysis
Energy balance
Metabolic engineering

ABSTRACT

Pseudomonas putida, a microbial host widely adopted for metabolic engineering, processes glucose through convergent peripheral pathways that ultimately yield 6-phosphogluconate. The periplasmic gluconate shunt (PGS), composed by glucose and gluconate dehydrogenases, sequentially transforms glucose into gluconate and 2-ketogluconate. Although the secretion of these organic acids by *P. putida* has been extensively recognized, the mechanism and spatiotemporal regulation of the PGS remained elusive thus far. To address this challenge, we adopted a dynamic ^{13}C- and ^{2}H-metabolic flux analysis strategy, termed *D-fluxomics*. D-fluxomics demonstrated that the PGS underscores a highly dynamic metabolic architecture in glucose-dependent batch cultures of *P. putida*, characterized by hierarchical carbon uptake by the PGS throughout the cultivation. Additionally, we show that gluconate and 2-ketogluconate accumulation and consumption can be solely explained as a result of the interplay between growth rate-coupled and decoupled metabolic fluxes. As a consequence, the formation of these acids in the PGS is inversely correlated to the bacterial growth rate—unlike the widely studied overflow metabolism of *Escherichia coli* and yeast. Our findings, which underline survival strategies of soil bacteria thriving in their natural environments, open new avenues for engineering *P. putida* towards efficient, sugar-based bioprocesses.

1. Introduction

Glycolysis, the biochemical process that converts glucose into pyruvate (Pyr, or other simple intermediates), constitutes a central part of cellular metabolism and is broadly distributed in all domains of Life (Escobar-Turriza et al., 2019; Romano and Conway, 1996). Multiple biochemical strategies for glycolysis exist in Nature, yet our view and understanding of sugar processing are still largely dominated by the metabolic architecture found in *Escherichia coli* and *Saccharomyces cerevisiae*. In these model organisms, glucose is channeled primarily through the linear Embden-Meyerhof-Parnas (EMP) pathway towards Pyr formation (Bar-Even et al., 2012; de Kok et al., 2012). However, understanding glucose catabolism in non-canonical bacterial hosts (Calero and Nikel, 2019) is of paramount interest to engineer efficient sugar consumption pathways (Wang and Yan, 2018)—an aspect that has largely relied on manipulating the EMP route thus far. Indeed, the Entner-Doudoroff (ED) and the pentose phosphate (PP) pathways (or variations thereof) prevail as the main sugar catabolic route in microorganisms that live in diverse, often-changing environmental niches (Chavarría et al., 2013; Chen et al., 2016; del Castillo et al., 2007; Flamholz et al., 2013; Klingner et al., 2015).

A distinct metabolic architecture ultimately leading to Pyr formation is the periplasmic gluconate shunt (PGS). *Pseudomonas* species, acetic acid bacteria and other microorganisms use these peripheral sugar oxidation routes, which generate gluconate and/or 2-ketogluconate (2KG) from glucose (del Castillo et al., 2007; Dolan et al., 2020; Latrach-Tlemçani et al., 2008; Matsushita et al., 2003). A peculiar feature of the PGS is that energy generation does not require active substrate uptake, unlike EMP-based sugar processing (Koebmann et al., 2002). Instead, the oxidation of glucose by glucose 2-dehydrogenase (Gcd) in the PGS is directly coupled to the reduction of pyrroloquinoline quinone (PQQ) electron-carriers, while the oxidation of gluconate to 2KG is accompanied by the reduction of flavin adenine dinucleotide (FAD) (Bachmann et al., 2013; Pfeiffer et al., 2001). Further oxidation of both redox cofactors during respiration yields adenosine triphosphate (ATP, with a different yield depending on the route), thus fueling the

* Corresponding author. The Novo Nordisk Foundation Center for Biosustainability, Technical University of Denmark, Lyngby, Denmark.
** Corresponding author. The Novo Nordisk Foundation Center for Biosustainability, Technical University of Denmark, Lyngby, Denmark.
E-mail addresses: chdavo@biosustain.dtu.dk (D.C. Volke), pabnik@biosustain.dtu.dk (P.I. Nikel).

https://doi.org/10.1016/j.ymben.2023.07.004
Received 16 May 2023; Received in revised form 30 June 2023; Accepted 13 July 2023
Available online 16 July 2023

cell's energy metabolism (Russell and Cook, 1995; Unden and Bongaerts, 1997). The presence of the PGS in several species underscores an ecological role for microbes thriving in their natural habitats, and gluconate excretion has been associated to gut colonialization and as a signal triggering toxin synthesis (Amirmozafari and Robertson, 1993; Sweeney et al., 1996). Some bacteria even shape the surrounding environment through gluconate secretion, as the acid helps solubilizing essential nutrients, thereby increasing their bioavailability (Buch et al., 2008; Sashidhar and Podile, 2010). Besides its ecological importance, the PGS has important implications for industrial fermentations and bioprocess engineering. *P. putida*, a soil bacterium widely adopted for metabolic engineering (Bitzenhofer et al., 2021; Weimer et al., 2020), favors glucose processing through the PGS (Vicente and Cánovas, 1973a, 1973b), yet the actual contribution of periplasmic oxidation reactions to the overall flux distribution has been merely estimated based on indirect experimental evidence.

The limited knowledge on these glycolytic strategies largely stems from a dearth of analytical tools to study the dynamics of periplasmic sugar processing. Metabolic flux analysis (MFA) provides valuable insight into which pathways are active and how carbon fluxes are distributed in a number of biological systems (Kohlstedt et al., 2010; Orth et al., 2010; Zamboni et al., 2009). Nonetheless, most MFA methodologies are heavily tailored for metabolic architectures found in *E. coli* and *S. cerevisiae* (Niedenführ et al., 2015). Adapting MFA techniques to other biological systems is a relatively straightforward task—provided that the metabolic blocks are conserved in the species of interest (Schwechheimer et al., 2018). An interesting exception is the cyclic glycolysis of environmental bacteria, i.e. the EDEMP cycle (Nikel et al., 2015), which comprises elements of the EMP, ED and PP pathways. Labeling information for metabolites derived from glucose-6-phosphate (G6P) and fructose-6-phosphate (F6P), in addition to the labeling information in proteinogenic amino acids, is needed to resolve EDEMP fluxes (Kohlstedt and Wittmann, 2019). Similarly, the PGS presents a significant challenge to traditional MFA approaches due to several reasons. Firstly, conversion of glucose to gluconate and/or 2KG does not involve any carbon atom transition. Thus, the pattern of carbon labeling in downstream metabolites does not provide information about which pathway(s) gave rise to them. Indeed, in previous MFA studies of *P. putida*, the PGS fluxes could only be inferred by indirect measurement of enzyme activities *in vitro* (Kohlstedt and Wittmann, 2019; Nikel et al., 2015, 2021). Secondly, the concentrations of gluconate and 2KG are not in a *pseudo*-steady state, but they rather fluctuate during bacterial growth—leading to a substantial (yet temporary) accumulation of these organic acids in batch cultures. Therefore, a singular time-point measurement captures only a snapshot of the fluxes and generates limited information about flux dynamics over time (Allen and Young, 2020).

To solve the long-standing question on the metabolic role of the PGS in *P. putida*, we have developed an MFA protocol (termed *D-fluxomics*), based on a combination of ^{13}C and ^{2}H-labeled substrates. ^{2}H has been previously employed as tracer in mammalian cells (Bednarski et al., 2021; Fan et al., 2014), and in specific applications in microbial cultures, e.g. to investigate acetate assimilation in an anammox bacterium (Lawson et al., 2021) and for deciphering the interplay between NADPH and lipid metabolism in aerobic heterotrophs (Wijker et al., 2019). We have identified ^{2}H (deuterium, D) as an ideal isotopic tracer to follow the fate of glucose in the upper sugar processing routes of *Pseudomonas*. Time-course experiments during batch cultivation on glucose and gluconate elucidated the spatiotemporal flux distribution through the different oxidation routes, in a first-case example of precise determination of PGS fluxes. The D-fluxomics approach revealed a hierarchical and highly dynamic uptake of different sugar forms, with rapid shifts between these substrates in a concentration-dependent fashion. Furthermore, we show that the temporal accumulation of gluconate and 2KG is inversely correlated to the growth rate and that this behavior can be solely explained by a model where the PGS flux is decoupled from bacterial growth. Thus, fluxes through peripheral oxidation steps decrease with faster growth—contrary to the traditional view of overflow metabolism. The impact of these findings on metabolic engineering efforts is discussed at the light of adopting sugars as the main feedstock for *Pseudomonas* fermentations.

2. Experimental procedures

2.1. Bacterial strains, mutant construction and culture conditions

Pseudomonas putida KT2440 (Bagdasarian et al., 1981) and its mutant derivatives were cultivated at 30°C. For standard applications, routine cloning procedures and during genome engineering manipulations, cells were grown in LB medium (containing 10 g L^{-1} tryptone, 5 g L^{-1} yeast extract and 10 g L^{-1} NaCl, pH = 7.0) (Sambrook and Russell, 2001). For all other experiments, *P. putida* was grown in de Bont minimal medium (Hartmans et al., 1989) supplemented with glucose or gluconate at the concentrations indicated in the text. If not stated otherwise, chemicals were supplied by Sigma-Aldrich Co. (St. Louis, MO, USA); [^{13}C–U]-glucose and [2-^{2}H]-glucose was purchased from Cambridge Isotope Laboratories Inc. (Tewksbury, MA, USA). *P. putida* Δ*glk* Δ*gtsABCD* Δ*gnuK* Δ*gntT* was created by marker-less, sequential deletion of the open reading frames of *glk*, *gtsABCD*, *gnuK* and *gntT* in wild-type strain KT2440 through homologous recombination (Volke et al., 2020; Wirth et al., 2020). Further deleting *gad* (encoding gluconate 2-dehydrogenase) in this genomic background using the same methodology, yielded *P. putida* Δ*glk* Δ*gtsABCD* Δ*gnuK* Δ*gntT* Δ*gad*. Finally, *P. putida* Δ*pgi-I* Δ*pgi-II*, a strain devoid of all phosphoglucoisomerase activity, was created by marker-less elimination of *pgi-I* and *pgi-II* in *P. putida* KT2440. All deletions were confirmed by PCR amplification of the corresponding loci followed by DNA sequencing of the amplicons (Fernández-Cabezón et al., 2021).

2.2. General protocol for time-resolved D-fluxomics

For high-precision quantitative physiology and labeling experiments, *P. putida* strains were grown in 50 mL of de Bont minimal medium (Hartmans et al., 1989) supplemented with glucose or gluconate in a temperature-controlled, 200-mL vessel and agitated with a magnetic stirrer or in 250-mL baffled Erlenmeyer flasks as specified in the text. In all cases, the medium was inoculated with an overnight culture grown in the same conditions to an optical density measured at 600 nm (OD_{600}) of ca 0.05 if not differently indicated. Samples were periodically withdrawn for determining OD_{600} values (in a 6705 UV/VIS scanning spectrophotometer; Jenway, Herlev, Denmark), concentration of sugars in the culture supernatants by HPLC (Nikel et al., 2016) and to analyze the labeling pattern in relevant metabolic intermediates (as explained in the next section). Growth rates in quantitative physiology experiments were calculated using the QurvE software (Wirth et al., 2023).

2.3. Metabolite extraction and measurement of isotopologue composition

At selected time points, 1-mL culture aliquots were withdrawn and vacuum-filtered (Durapore™ membrane filter, 0.45 μm; Sigma-Aldrich Co.). Upon filtration, the filter was re-extracted with 1 mL of acetonitrile/methanol/water [in a 40/40/20% (v/v) ratio] acidified with 0.1 M formic acid at −20 °C (Rabinowitz and Kimball, 2007). Subsequently, cell debris were removed by centrifugation at 17,000×*g* for 2 min at 4 °C. The supernatant was transferred to a new tube and solvents were removed by evaporation at 30 °C for 90 min at reduced pressure (Concentrator Plus; Eppendorf SE, Hamburg, Germany). The samples were then fully dried in a freeze-dryer and stored at −80 °C (Wirth et al., 2022). Prior to the analysis, the samples were reconstituted in 100 μL of HPLC-grade H_2O. The metabolites were analyzed using a Prominence XR (Shimadzu Corp., Columbia, MD, USA) HPLC system coupled to a 5500 QTRAP mass spectrometer (SciEx, Framingham, MA, USA). The autosampler was cooled to 15 °C. A sample of 10 μL was injected and

separated in an XSelect HSS T3 150 × 2.1 mm^2 × 2.5 μm column (Waters Corp., Milford, MA, USA). The column temperature was held at 40 °C; metabolites were eluted with a constant flow rate of 0.4 mL min^{-1}. Elution began with 100% buffer A [10 mM tributylamine, 10 mM acetic acid (pH = 6.86), 5% (v/v) methanol and 2% (v/v) 2-propanol]. Starting at 4 min, buffer B (2-propanol) was linearly increased to 15% at 8 min and held at 15% at 12 min. Buffer B was then linearly decreased to 0% at 13.5 min and kept at 0% until 17 min. The mass spectrometer was operated in negative mode with multiple reaction monitoring, and unit resolution for the mass filters Q1 and Q3 was used for detection and quantification. The parameters and settings used for electrospray ionization were as following: electrospray voltage, −4500 V; temperature, 500 °C; curtain gas, 40 pound square $inch^{-1}$ (psi); CAD gas, 12 psi; gas 1 and 2, 50 psi each; and collision gas, high. Detection parameters were optimized for each metabolite, together with the expected transitions when in isotopic labelling experiments (Table S1 in the Supplementary Material).

2.4. Flux ratio analysis based on ^{13}C- and ^{2}H-isotopic tracers

A system of 15 equations, indicated as v_1-v_{15} and comprising reactions of the (incomplete) EMP, ED and PP pathways of *P. putida*, was used to resolve the distribution of fluxes within the PGS in *P. putida*. The metabolic network adopted for MFA, together with a list of the enzymes annotated to catalyze the corresponding reactions in *P. putida* KT2440, is shown in Fig. 1. The first step was calculating φ_{G6P}, the fraction of the G6P pool originating from glucose (abbreviated as Glu in the equations below). This parameter was calculated using either the m+3 or m+6 isotopologue fraction in labeling experiments fed with [U–^{13}C]-glucose or the m+1 isotopologue fraction when [2-^{2}H]-glucose was used as the carbon source, as indicated in **Equation (1)**.

$$\varphi_{G6P} = \frac{v_1}{v_1 + v_{10}} = \frac{G6P^{m+x} - F6P^{m+x}}{Glu^{m+x} - F6P^{m+x}} \quad (1)$$

It was further assumed that all flux from G6P is directed towards the formation of 6-phosphogluconate (6PG), as shown in **Equation (2)**.

$$v_2 = v_1 + v_{10} \quad (2)$$

The fraction of 6PG originating form G6P (φ_{6PG}) was calculated using the m+3 or m+6 isotopologue fraction in experiments with [U–^{13}C] (**Equation (3)**), assuming that the isotopologue fraction in glucose, gluconate (Gln) and 2KG of m+3 and m+6 is equal.

$$\varphi_{6PG} = \frac{v_2}{v_2 + v_3 + v_5} = \frac{6PG^{m+x} - Glu^{m+x}}{G6P^{m+x} - Glu^{m+x}} \quad (3)$$

The fractional contribution of each isotopologue to the 6 PG pool is given by **Equation (4)**.

$$6PG^{m+3} = \frac{G6P^{m+x} \times v_2 + Gln^{m+x} \times v_3 + 2KG^{m+x} \times v_5}{v_2 + v_3 + v_5} \quad (4)$$

Fixing the total inflow into 6PG to 1 results in **Equation (5)** and **Equation (6)** for flux originating from gluconate,

$$v_5 = \frac{6PG^{m+x} - G6P^{m+x} \times v_2 - Glu^{m+x} + Glu^{m+x} \times v_2}{2KG^{m+x} - Glu^{m+x}} \quad (5)$$

or from 2KG, *via* 2-keto-6-phosphogluconate (2K6PG).

$$v_3 = \frac{6PG^{m+x} - G6P^{m+x} \times v_2 - 2KG^{m+x} + 2KG^{m+x} \times v_2}{Glu^{m+x} - 2KG^{m+x}} \quad (6)$$

As it can be noted in the denominator of **Equations 5 and 6**, the system is solvable only if the isotopologue fraction in Glu and 2KG differ from each other. Therefore, the m+1 isotopologue fraction was used in experiments with [2-^{2}H]-glucose as the carbon source for calculating the v_3 and v_5 fluxes.

2.5. Quantification of the glucose, gluconate and 2-ketogluconate concentrations

An aliquot of 100-μL was withdrawn from the cultures at the indicated time-points. The samples were centrifuged at 13,000×*g* for 5 min at 4 °C and the supernatant was transferred to a new tube. Subsequently, 20 μL of the supernatant were injected onto an Aminex HPX-87H (300 ×

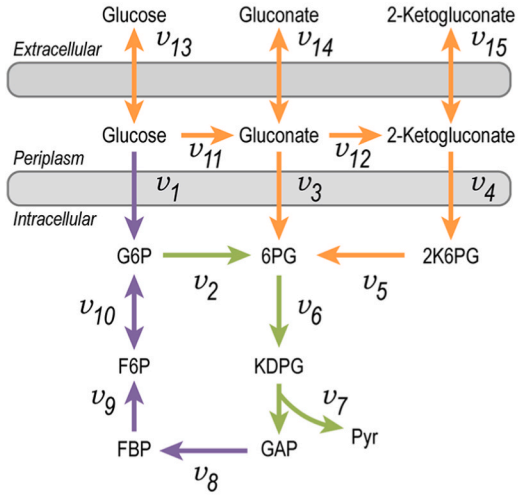

Functional block	Flux code	Enzyme(s)	Names and PP numbers of coding gene(s)
Embden-Meyerhof-Parnas pathway	1	Glucose ABC transporter	*gtsABCD* (PP_1015-PP_1018)
		Glucose kinase	*glk* (PP_1011)
	8	Triose-*P* isomerase	*tpiA* (PP_4715)
		Fructose-1,6-bisphosphate aldolase	*fba* (PP_4960)
	9	Fructose-1,6-bisphosphatase	*fbp* (PP_5040)
	10	Glucose-6-phosphate isomerase	*pgi-I* (PP_1808), *pgi-II* (PP_4701)
Entner-Doudoroff pathway	2	Glucose-6-phosphate 1-dehydrogenase	*zwfA* (PP_1022), *zwfB* (PP_4042)
	7	2-Keto-3-deoxy-6-phosphogluconate aldolase	*eda* (PP_1024)
	6	6-Phosphogluconate dehydratase	*edd* (PP_1010)
Peripheral glucose oxidation pathway	11	Glucose dehydrogenase	*gcd* (PP_1444)
	12	Gluconate dehydrogenase	*gad* (PP_3382-3384)
	13	Carbohydrate selective porine	*oprB-I* (PP_1019), *oprB-II* (PP_1445), *oprB-III* (PP_3570)
	14	Basic amino acid-specific porin	*oprD* (PP_1206)
	15	2-Ketogluconate exporter	N.I.
	3	Gluconate transporter	PP_0652, PP_3074, *gntT/P* (PP_3417)
		Gluconate kinase	*gnuK* (PP_3416)
	4	2-Ketogluconate transporter	*kguT* (PP_3377)
		2-Ketogluconate kinase	*kguK* (PP_3378)
	5	2-Ketogluconate-6-phosphate reductase	*kguD* (PP_3376)

Fig. 1. Metabolic network used for calculating the flux distribution within the upper sugar metabolism of *P. putida*. The enzymes catalyzing the fluxes indicated and the genes encoding them are listed in the table; the information was compiled from the *Pseudomonas* Genome Database (Winsor et al., 2016), MetaCyc (Caspi et al., 2018) and the literature (Belda et al., 2016; Nogales et al., 2020). In the instances in which no gene name has been assigned, the PP number is given for each open reading frame; biochemical reactions are coded according to the three functional blocks indicated in the figure and some reactions are lumped for the sake of simplicity (e.g. Zwf and Pgl in v_2). Abbreviations: G6P, glucose-6-phosphate; F6P, fructose-6-phosphate; FBP, fructose-1,6-bisphosphate; 6PG, 6-phosphogluconate; KDPG, 2-keto-3-deoxy-6-phosphogluconate; 2K6PG, 2-keto-6-phosphogluconate; GAP, glyceraldehyde-3-phosphate; Pyr, pyruvate; *N.I.*, not identified.

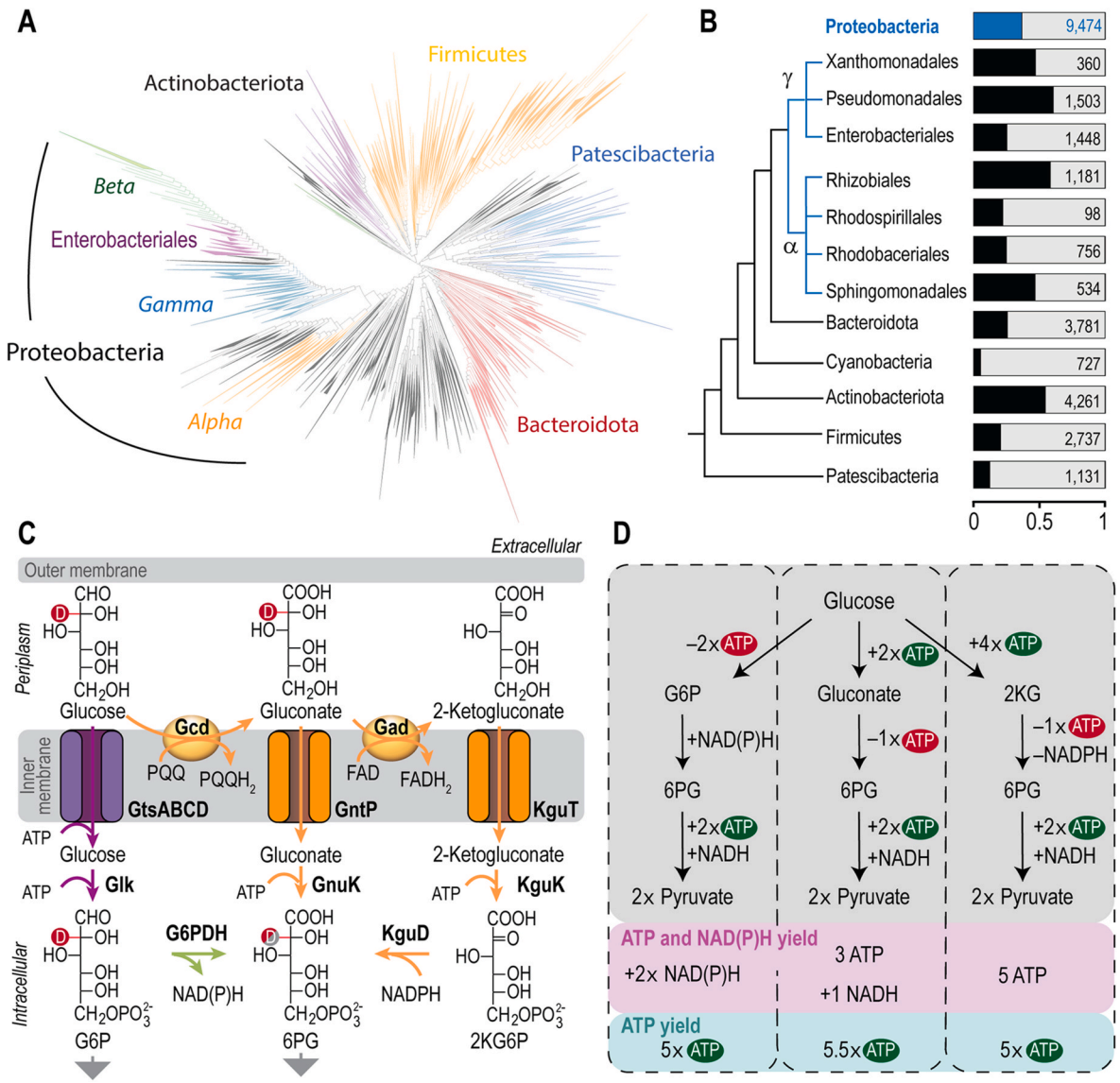

Fig. 2. Phylogenetic distribution and stoichiometric analysis of the periplasmic oxidation shunt. (A) Phylogenetic distribution of a periplasmic gluconate shunt in the bacterial kingdom. The presence of a pyrroloquinoline quinone (PQQ)-dependent glucose dehydrogenase (Gcd) was adopted as a proxy for the analysis, with a wide distribution over all phyla (overall, 31% of all bacterial species carry a Gcd polypeptide). **(B)** Main phyla and orders of bacteria harboring Gcd. Both the relative fraction of Gcd-containing bacteria and the total number of species analyzed in each phyla or order are indicated in the diagram; Proteobacteria (α and γ) are highlighted in blue. **(C)** Glucose processing through either its direct phosphorylation or periplasmic, sequential oxidation in *P. putida*. Glucose can be directly taken up and phosphorylated to glucose-6-phosphate (G6P) by an ATP-dependent glucose transporter (GtsABCD) and glucose kinase (Glk), respectively. The hexose can be also oxidized to gluconate *via* glucose dehydrogenase (Gcd). Similarly, gluconate can be transported by a gluconate permease (GntP) and either phosphorylated by gluconokinase (GnuK) to 6-phosphogluconate (6PG) or oxidized to 2-ketogluconate through a flavin adenine dinucleotide (FAD)-dependent gluconate dehydrogenase (Gad). Finally, 2-ketogluconate is imported to the bacterial cytoplasm and phosphorylated to 2-keto-6-phosphogluconate (2K6PG) by means of the 2-ketogluconate transporter (KguT) and a 2-ketogluconate kinase (KguK), respectively. Note that deuterium (D, indicated as a red circle) at position two in the glucose molecule would remain unaffected during glucose and gluconate uptake; however, gluconate oxidation to 2-ketogluconate releases the deuterium label (see also Fig. 3). Therefore, the 6PG pool will be differentially labeled depending on which sugar uptake routes are active. Grey arrows indicate further processing of key intermediates into central carbon metabolism. **(D)** Formation and consumption of ATP and soluble reducing equivalents [i.e. NAD(P)H] through the different catabolic routes of glucose to pyruvate. The ATP yield *via* Gad processing was estimated based on the translocation of 4 H^+ (Simon et al., 2008).

7.8 mm, 9 μm; Bio-Rad Laboratories Inc., Hercules, CA, USA). The sample was eluted over 30 min at 30 °C with 5 mM H_2SO_4 at a constant flow of 0.6 mL min^{-1} (Nikel et al., 2009). Refraction index (RI) was used for the quantification of co-eluted glucose and gluconate, while absorbance at 205 nm was used to quantify gluconate and 2KG. The calculated RI of gluconate was subtracted from the detected gluconate + glucose signal to obtain the actual RI of glucose (Nikel et al., 2015; Pedersen et al., 2021). Authentic standards were used to construct calibration curves for all relevant sugars.

2.6. Preparation of [2-^{2}H]-labeled gluconate from deuterated glucose with resting *P. putida* cells

P. putida Δ*glk* Δ*gtsABCD* Δ*gnuK* Δ*gntT* Δ*gad* was grown in 100 mL of de Bont minimal medium supplemented with 0.4% (w/v) succinate placed in a 500-mL baffled Erlenmeyer flask. After reaching stationary phase (ca. 18 h), cells were harvested by centrifugation at 5000×*g* for 10 min at room temperature. The bacterial sediment was suspended in 10 mL of de Bont minimal medium without carbon source, followed by an additional centrifugation step at 5000×*g* for 10 min. Then, cells were

suspended in 50 mL of de Bont minimal media with the mixture of labeled glucose specified in the text, transferred to a 500-mL baffled Erlenmeyer flask and incubated with constant shaking at 30 °C. Periodically, 1-μL aliquots were withdrawn from the culture and quickly tested for residual glucose (semi-quantitative QuantoFix™ test strips; Macherey-Nagel, Düren, Germany) and pH (pH-fix 0–14 indicator strips; FischerBrand, Langenselbold, Germany). If needed, the pH was adjusted to 7.5–8 by dropwise addition of 5 M NaOH, and the transformation was continued until no residual glucose was detected. Next, the suspension was centrifuged at 5000×*g* for 10 min, the supernatant was transferred to a new 50-mL Falcon tube (Sigma-Aldrich Co.) and centrifuged at 12,000×*g* for 10 min. Finally, the supernatant was transferred to a clean tube and filter-sterilized by passing through a 0.45-μm membrane (Sigma-Aldrich Co.). Gluconate and (residual) glucose were detected and quantified by HPLC as explained above.

2.7. Modelling bacterial growth and extracellular metabolite concentration during batch cultivation of *P. putida*

The changes of metabolites in the supernatant over time are given by Equation (7), (8) and (9).

$$\frac{d[Glu]}{dt} = r_{Gcd} - r_{Gad} - r_{GnuK} \tag{7}$$

$$\frac{d[Gln]}{dt} = -r_{Gcd} - r_{Glk} \tag{8}$$

$$\frac{d[2KG]}{dt} = r_{Gad} - r_{KguK} \tag{9}$$

$[Glu]$, $[Gln]$ and $[2KG]$ represent the concentration of glucose, gluconate and 2KG, respectively, while r_Z is the conversion rate through enzyme Z. For all enzymatic steps, a Michaelis-Menten kinetic was assumed (Zotter et al., 2017). The rates through the Gad and Gcd reactions were calculated through the specific maximal activity (V^X_{max}) and the biomass concentration ($[X]$) as indicated in **Equations 10** and **11**, respectively.

$$r_{Gcd} = V^{Gcd}_{max}\frac{[Glu]}{[Glu] + K^{Gcd}_M}[X] \tag{10}$$

$$r_{Gad} = V^{Gad}_{max}\frac{[Gln]}{[Gln] + K^{Gad}_M}[X] \tag{11}$$

Therefore, no coupling to the growth rate (μ) was assumed for these calculations. In contrast, the uptake rate through the different pathways under consideration was assumed to be proportional to the growth rate, as enunciated in Equation (12), **13** and **14**.

$$r_{Glk} = f_{Glk}\frac{1}{Y_{Glu}}[X]\mu \tag{12}$$

$$r_{GnuK} = f_{GnuK}\frac{1}{Y_{Gln}}[X]\mu \tag{13}$$

$$r_{KgnuK} = f_{KguK}\frac{1}{Y_{2KG}}[X]\mu \tag{14}$$

where Y_Z is the yield on substrate Z and f_Z is the relative fraction of total carbon source entering through the enzymatic step Z. The fractional uptake was given by the empirically-determined uptake distribution D under saturation conditions normalized to the relative saturation of each uptake with its substrate S (**Equation (15)**).

$$f_Z = D_Z\frac{[S_Z]}{[S_Z] + K^Z_M}\sum_i\frac{[S_i]}{[S_i] + K^i_M}\, i, x = \{Glk, GnuK, KguK\} \tag{15}$$

The biomass concentration was determined by **Equation (16)**.

$$[X] = X_o e^{\mu t} \tag{16}$$

where X_0 is the initial biomass.

Simulations were carried out with different growth rates, initial values of biomass, glucose concentration and altering kinetic parameters as indicated in the text. In all cases, at least 2000 iterative steps were carried out with time steps between 0.001 and 0.0035 h.

2.8. Phylogeny distribution of the periplasmic gluconate shunt across the tree of life

Information on orthologues to Gcd (K00117; EC 1.1.5.2) and Gad (K05308; EC 4.2.1.140) was retrieved from KEGG (Kanehisa et al., 2022) through AnnoTree (Mendler et al., 2019). The minimum identity for the search was set to 30%, while subject and query alignment were fixed to 70 and maximum E value to 0.00001, respectively. The resulting phylogenetic tree was drawn with the *i*TOL package (Letunic and Bork, 2021).

2.9. Data and statistical analysis

All experiments reported in this study were independently repeated at least twice (as indicated in the corresponding figure legend), and the mean value of the corresponding parameter ± standard deviation is presented. Whenever relevant, the level of significance of the differences when comparing results was evaluated by means of the Student's *t*-test with $\alpha = 0.01$ or $\alpha = 0.05$ as indicated in the figure legends.

3. Results and discussion

3.1. The periplasmic gluconate shunt, widely distributed in the bacterial kingdom, underscores energy and redox versatility

The PGS reactions have been recognized as the predominant sugar processing mechanism in *Pseudomonas* and related rhizobacteria a long time ago (Vicente and Cánovas, 1973b)—yet the extent of its presence in Nature remains unsolved. To gain insight into the distribution of the PGS across multiple species in the bacterial kingdom, we selected the Gcd and Gad enzymes as a proxy for the presence of these two oxidation steps. The resulting phylogenetic reconstruction indicated that the PGS is indeed widely distributed in bacterial species (Fig. 2A). The PPQ-dependent glucose dehydrogenase (Gcd) is found in 31% of all bacterial species, with an uneven distribution over the different phyla (i.e. Actinobacteria, Firmicutes, Patescibacteria, Bacteroidota and Proteobacteria). The Actinobacteriota and Proteobacteria phyla are especially enriched in species harboring the PGS (Fig. 2B). Inside the Proteobacteria phylum (and out of the 9474 members analyzed herein), the Pseudomonadales and Rhizobiales orders have the highest density of Gcd-bearing species. Indeed, the fraction of Gcd-containing species accounted for >0.45 of all γ-Proteobacteria (i.e. Pseudomonadales and Rhizobiales) and Actinobacteria analyzed. In contrast, Cyanobacteria had the lowest abundance of Gcd-bearing species (Fig. 2B). The second step in the PGS, catalyzed by gluconate dehydrogenase (Gad), was present in ca. 8% of all bacterial genomes used in this analysis, roughly following the same distribution trend as observed for Gcd—albeit at a significantly lower frequency (details not shown). The uneven distribution of the PGS in the bacterial kingdom may be connected to some intrinsic characteristics of this metabolic feature. Firstly, gluconate cannot be metabolized through the linear EMP pathway. Thus, bacteria exclusively adopting the EMP pathway for glycolysis do not usually have an active PGS metabolism (Eisenberg and Dobrogosz, 1967). Secondly, the synthesis of the PQQ cofactor is strictly oxygen-dependent (An and Moe, 2016), which indicates that the presence of a PQQ biosynthesis pathway is largely restricted to either aerobic microorganisms or those dwelling in environments where PQQ is available (Zhu and Klinman, 2020). Interestingly, the abundance of the PGS feature in bacteria correlates well with the phylogenetic distribution of the ED catabolic route (Chavarría et al., 2013; Volke et al., 2021) and the presence of a PQQ biosynthesis pathway (Zhu and Klinman, 2020) over all the phyla.

To understand the metabolic function of the PGS, it is worth to analyze the stoichiometry and the energy and redox yields of these routes in detail. The PGS directly couples the oxidation of glucose and gluconate to the respiratory chain. In particular, the oxidation of glucose to glucono-δ-lactone, an intermediate that spontaneously hydrolyses to gluconate, drives PQQ reduction to $PPQH_2$, while the oxidation of gluconate to 2KG is coupled to FAD reduction to $FADH_2$ (Fig. 2C). Both reduced cofactors subsequently transfer the electrons to ubiquinol,

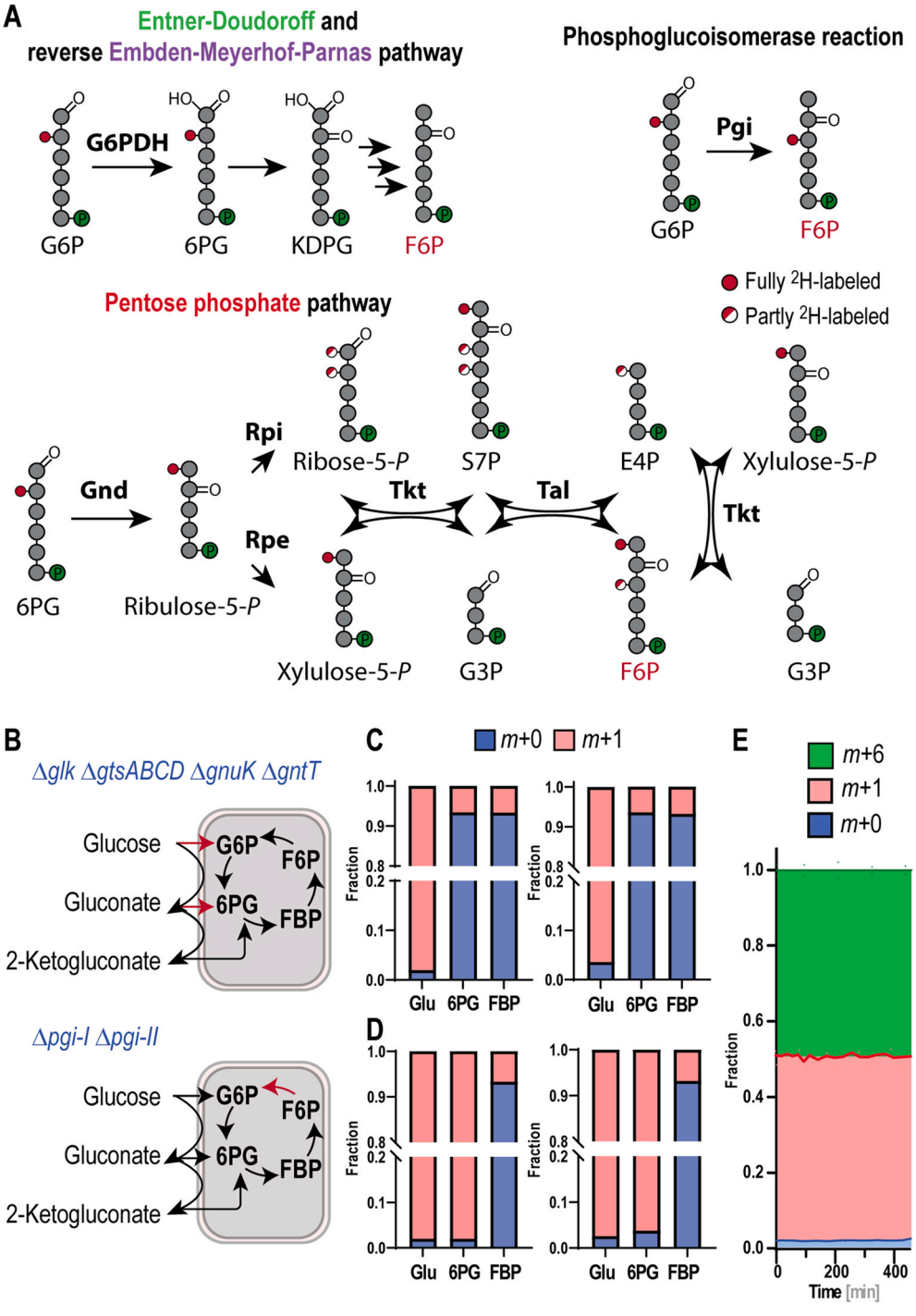

Fig. 3. Deuterium transition maps and experimental validation of D-fluxomics in *P. putida* grown on [2-^{2}H]-glucose. **(A)** Atomic transitions through the Entner-Doudoroff (ED) pathway, the reverse (i.e. gluconeogenic) Embden-Meyerhof-Parnas (EMP) pathway and the pentose phosphate (PP) pathway. The deuterium (D, ^{2}H) label is lost in the ED catabolism during the oxidation of 6-phosphogluconate (6PG) to 2-keto-3-deoxy-6-phosphogluconate (KDPG). In the EMP pathway, [2-^{2}H]-glucose-6-phosphate (G6P) can be converted into [3-^{2}H]-fructose-6-phosphate (F6P) by the action of phosphoglucoisomerase (G6P isomerase, Pgi). In contrast, labeling transitions in intermediates of the PP pathway are more complex and enzyme-dependent. Glyceraldehyde-3-phosphate (G3P) remains unlabeled regardless of the enzyme activities involved in 6PG processing, while F6P is D-labeled in position C1 and, depending on its metabolic origin, also in position C3. In all cases, the D signal is marked with a red dot; if the probability of finding a D label in the annotated position is 50%, the dot is half filled. Abbreviations: G6PDH, G6P dehydrogenase; Gnd, 6PG dehydrogenase; Rpe, ribulose-5-phosphate 3-epimerase; Rpi, ribulose-5-phosphate isomerase; Tkt, transketolase; Tal, transaldolase; S7P, sedoheptulose-7-phosphate; and E4P, erythrose-4-phosphate. **(B)** Strains used for experimental validation of D-fluxomics. *P. putida* Δ*glk* Δ*gtsABCD* Δ*gnuK* Δ*gntT* cannot take up glucose or gluconate, but this strain is still able to oxidize glucose to 2-ketogluconate, which is transported and processed to 6PG (upper panel). Deletion of the two phosphoglucoisomerase genes of *P. putida* (i.e. *pgi-I* and *pgi-II*) interrupts carbon cycling in the EDEMP cycle (lower panel). The missing reactions in the mutant *P. putida* strains are indicated with red arrows. **(C)** Theoretical and experimentally-determined D-label patterns (left and right panel, respectively) for glucose (Glu), 6PG and fructose-1,6-bisphosphate (FBP) when *P. putida* Δ*glk* Δ*gtsABCD* Δ*gnuK* Δ*gntT* was grown on 100% [2-^{2}H]-glucose. The isotopologue fractions *m*+0 (containing no heavy isotope) and *m*+1 (containing one heavy isotope) of these metabolites is shown. **(D)** Theoretical and experimentally-determined isotopologue patterns (left and right panel, respectively) for glucose (Glu), 6PG and fructose-1,6-bisphosphate (FBP) calculated and determined when *P. putida* Δ*pgi-I* Δ*pgi-II* was grown on 100% [2-^{2}H]-glucose. **(E)** Fractional labelling of glucose throughout a batch fermentation of wild-type *P. putida* KT2440. In these experiments, the initial isotope tracer composition was 50% [U–^{13}C]-glucose and 50% [2-^{2}H]-glucose. The *m*+0, *m*+1 and *m*+6 fractions of the glucose pool are individually indicated; all experiments represented in the figure were repeated in independent biological triplicates.

which allows for the direct translocation of two protons (Sone et al., 2010). In contrast, the oxidation of ubiquinone, the reduced form of ubiquinol, enables the translocation of six protons through the complexes III and IV in the respiratory chain. Taken together, these steps yield eight translocated protons—while the oxidation of NAD(P)H, the redox currency formed in the alternative, cytoplasmic and ATP-dependent sugar oxidation, results in the translocation of ten protons through complexes I, III and IV in the respiratory chain. Assuming that four protons drive the synthesis of one ATP molecule, the metabolic route that proceeds through G6P dehydrogenase (G6PDH) and 2K6PG reductase (KguD) yields 5 ATP equivalents, while the direct phosphorylation of gluconate yields 5.5 ATP (Fig. 2D). Even though the ATP yields are in principle similar, the balance of redox cofactors in the cell differs significantly. While the uptake of glucose and further processing to 6PG produces NAD(P)H (Volke et al., 2021), 2KG transport and conversion to 6PG consumes redox equivalents (Latrach-Tlemçani et al., 2008; Torrontegui et al., 1976)—while gluconate uptake (and direct phosphorylation to 6PG) is redox-neutral (Vicente et al., 1975). Such differences at the energy and redox balances probably confer metabolic flexibility to bacteria running these alternative glycolytic strategies in parallel (Dolan et al., 2022; Nikel et al., 2014; Wilkes et al., 2019)—without any significant protein expenditure. Motivated by these observations on the ubiquitous presence of the energy and redox versatile PGS-based metabolism in environmental bacteria, we adopted *P. putida* as a model system to explore the mechanistic details of glucose transport, oxidation and downstream catabolism as explained in the next section.

3.2. D-fluxomics: adopting [2-^{2}H]-glucose as an isotopic tracer for metabolic flux analysis

MFA methodologies have been adapted to analyze a broad range of organisms beyond *E. coli*, yeast and mammalian cells (Niedenführ et al., 2015). As indicated previously, novel challenges had to be solved prior to applying ^{13}C-based MFA in *P. putida* and related species. While glucose is metabolized through a linear EMP pathway in *E. coli* and yeast, rhizobacteria harbor a cyclic glycolytic catabolism (Nikel et al., 2015; Wilkes et al., 2019). In addition to this occurrence, the distribution of fluxes in the PGS cannot be fully elucidated with the currently available MFA methods (Kohlstedt and Wittmann, 2019)—owing to identical carbon transitions in the two branches of the PGS, which preclude labeling-based discrimination. To address this technical challenge, we evaluated ^{2}H-based MFA as an alternative methodology to elucidate fluxes through the PGS node. We started by evaluating the atomic transitions expected in the PGS if *P. putida* KT2440 were grown on [2-^{2}H]-glucose (Fig. 2C). The deuterium (D) label at position C2 of the sugar should be conserved in the reactions catalyzed by Glk, Gcd and GnuK, while the oxidation of gluconate to 2KG by Gad and its subsequent reduction by KguD would lead to the replacement of the D label by an H atom derived from water or NADPH (Fig. 2C). Therefore, the enrichment in deuterated 6PG relative to G6P should reflect the flux ratio through GnuK and KguK. Moreover, the pattern of D-labeling of F6P provides useful information on which glycolytic pathway gave rise to this metabolite (Fig. 3A). Indeed, the conversion of G6P into F6P by Pgi (phosphoglucoisomerase) does not affect the labeling in the C2 position, whereas D is lost when G6P is processed through the EDEMP cycle. When F6P is derived from 6PG through the PP pathway, the resulting labeling pattern corresponds to a mixed pool of D-containing and D-free F6P molecules. If the information based on D enrichment of these metabolites is combined with an orthogonal isotopic tracer, e.g. [U–^{13}C]-glucose, this methodology, termed *D-fluxomics*, should enable resolving all fluxes of carbon uptake and cycling through the EDEMP cycle.

In order to explore the metabolic H/D transitions *in vivo* and validating the D-fluxomics methodology, we constructed two mutants derived from *P. putida* KT2440 (Fig. 3B). In *P. putida* Δ*glk* Δ*gtsABCD* Δ*gnuK* Δ*gntT*, glucose can only be oxidized to gluconate or 2KG—but only 2KG, the most oxidized form of the sugar, can be transported into the cell and reduced to 6PG for further catabolism. In contrast, in the second mutant, the elimination of *pgi-I* and *pgi-II* blocks the interconversion of G6P and F6P, effectively interrupting cycling of hexoses phosphate within the EDEMP cycle. These strains were grown in shaken-flasks cultures using [2-^{2}H]-glucose as the only carbon source, and the labeling pattern of glucose, 6PG and FBP (i.e. the *m*+0 and *m*+1 pools for each metabolite) was determined during exponential growth (Fig. 3C and **D**). As predicted from the atomic transitions within the PGS (Fig. 2C), the D labeling in position C2 of glucose should be lost during carbon uptake *via* 2KG in *P. putida* Δ*glk* Δ*gtsABCD* Δ*gnuK* Δ*gntT*, with the intermediate pools reflecting the natural isotope abundance in the substrate. Indeed, growing the mutant strain on 100% [2-^{2}H]-glucose led to the expected labeling pattern in 6PG and FBP with a high accuracy level: the predicted *m*+1 fractions are 6.6 and 6.7%, and the experimentally measured fractions were 6.5% and 6.8% for 6GP and FBP, respectively (Fig. 3C). Hence, these experimental results confirm the proposed H/D transitions through the sequential activities of Gad and KguK (Fig. 2C). To check if the D-label is lost during carbon uptake at the level of glucose or gluconate (and their processing through Glk and GnuK), *P. putida* Δ*pgi-I* Δ*pgi-II* was likewise grown on [2-^{2}H]-glucose. As indicated above, knocking-out the phosphoglucoisomerase step prevents cycling through the EDEMP pathway, which would otherwise result in an increased fraction of unlabeled G6P and 6PG as the D in position C2 is eliminated in the dehydration of 6PG by Edd. Again, the experimentally-determined labeling pattern of extracted metabolites matched the theoretical prediction almost identically (Fig. 3D). In this case, the labeling of the G6P pool mirrored the labeling pattern in glucose, while the minor fraction of deuterated FBP could only be attributed to the natural isotopic abundance in the substrate.

While these results indicated the general validity of the D-fluxomics approach, a last concern was the stability and persistence of the [2-^{2}H]-glucose–dependent labeling in the metabolites, as spontaneous proton exchange reactions exist between carbohydrates and water (Lehmann, 2017; Li et al., 2016). To test whether this phenomenon could affect our experimental setup, a mixture of 50% [U–^{13}C]-glucose and 50% [2-^{2}H]-glucose was used as the only carbon substrate in shaken-flask cultivations of wild-type *P. putida* KT2440, and the isotopologue composition of the residual glucose was periodically monitored throughout the batch cultivation (Fig. 3E). We detected no noticeable changes in the isotopologue composition of glucose over time. This observation suggest that, on the one hand, the D label is stable during the timescale relevant for D-fluxomic experiments and, on the other hand, that there is no measurable discrimination of isotopologues by the enzymes involved in sugar uptake and oxidation in *P. putida*. Even when a slight preference against isotopes by some enzymes cannot be totally ruled out, such an effect has been deemed negligible for most tracer experiments (Low et al., 2023; Sandberg et al., 2016). The labeling strategy presented in this section satisfies all of the requirements needed to be adopted for metabolic flux analysis—hence, [2-^{2}H]-glucose was employed for elucidating sugar metabolism in *P. putida* as disclosed below.

3.3. Deploying D-fluxomics for high-resolution mapping of glucose processing in P. putida

3.3.1. Challenges in metabolic flux analysis of non-canonical sugar processing architectures

Thus far, MFA studies on *P. putida* and related species have been carried out essentially at single-time point measurements during exponential growth (de Oliveira et al., 2021; Fuhrer et al., 2005; Kohlstedt and Wittmann, 2019; Nikel et al., 2015, 2021; Wilkes et al., 2019). As indicated above, such procedures were adopted from methodologies that were originally designed for *E. coli* and yeast cultivations. In these model organisms, all metabolites reach a *quasi*-steady-state during exponential growth, except for the substrate, glucose, and secretion products, e.g. acetate, ethanol and CO_2 (Kelleher, 2001). Under these conditions, the

intracellular metabolite concentrations (hence, the producing and consuming fluxes) do not change over time. This assumption, however, does not hold true for *Pseudomonas*. In these species, gluconate and 2KG accumulate transiently in the culture medium throughout the cultivation on glucose, which indicates that the producing and consuming fluxes around these metabolites are different, changing over time. From a methodological point of view, this problem is compounded by the dearth of experimental data on the enrichment of gluconate and 2KG in the bacterial periplasm. Furthermore, the extensive lag phases observed in cultures of *P. putida* mutants defective in direct glucose utilization in the EDEMP cycle (Δ*zwfA* Δ*zwfB* Δ*zwfC*) or glucose and gluconate processing *via* phosphorylation (Δ*glk* and Δ*gnuK*, respectively) strongly suggest that *pseudo*-steady state concentrations for gluconate and 2KG are not immediately established in the periplasm (Volke et al., 2021). Furthermore, the primary literature reports significant differences in the flux distribution between sugar phosphorylation or oxidation. Such discrepancies range from 10% to 33% for direct glucose phosphorylation, while other fluxes vary much less between studies (Kohlstedt and Wittmann, 2019; Nikel et al., 2015). Taken together, the observations listed above gave rise to the hypothesis that the initial steps of glucose routing and processing in *P. putida* are dynamic, and probably dependent on the growth phase and oxygenation of the culture. Therefore, we aimed at capturing flux changes during batch cultivations by performing time-series measurements instead of single sampling points and integrating the data in the context of the D-fluxomics approach. Here, measuring the labeling pattern of glycolytic intermediates (instead of the customary protein-derived amino acids) is advantageous as the half-life time of these metabolites is much shorter (in the order of seconds to minutes)—therefore, they retain information on the metabolic fate of carbon atoms during short periods (Bilbao et al., 2023; Wishart, 2008). The labeling patterns of proteinogenic amino acids, in contrast, convey information of a longer period of biochemical processing. Building on these considerations, we adopted the D-fluxomics framework to obtain a detailed map of the glucose processing routes in *P. putida*.

3.3.2. Hierarchical uptake of glucose, gluconate and 2-ketogluconate by *P. putida* KT2440

In order to combine experimental data on quantitative physiology, biomass formation, accumulation of metabolites in culture supernatants, together with the actual flux distribution in glucose-grown *P. putida*, we followed the workflow outlined in Fig. 4A. To this end, wild-type *P. putida* KT2440 was cultured in de Bont minimal medium containing U–^{13}C, 2-^{2}H and unlabeled glucose; measurements were periodically taken in parallel for all relevant parameters. The starting cell density for these cultivations was set to an OD_{600} of 0.2. This fairly high amount of cells at the onset of the cultivation was deliberately chosen to ensure that sufficient biomass for metabolite extraction procedures would be available shortly after initiating the cultures—thereby capturing the metabolism in a state where glucose should be predominantly taken up and phosphorylated, rather than being oxidized to gluconate. The growth rate over the whole cultivation was essentially constant at $\mu = 0.68 \pm 0.05\ h^{-1}$, the (i.e. glucose, gluconate and 2KG) was $Y_{X/S} = 0.110 \pm 0.004\ g_{CDW}\ mmol^{-1}$ and the total carbon uptake rate was 6.2 ± 0.5 mmol $g_{CDW}^{-1}\ h^{-1}$ (Figs. S1A and S1B in the Supplementary Material), similar to previously reported values (Kohlstedt and Wittmann, 2019; Nikel et al., 2015). The first sampling was carried out after 9.6 min of initiating the cultivation and, even at this early time point, gluconate and 2KG were already present in the extracellular medium at 0.73 ± 0.05 mM and 0.18 ± 0.01 mM, respectively (Fig. 4B). This observation implies an extremely fast accumulation of these sugar metabolites in the early growth phase. Even though gluconate and 2KG were present at substantial, non-negligible quantities at this data point, the flux through Glk was more than twice as high (17% ± 4%) as compared to all of the later time points (6%–9%, Fig. 4C)—indicating a dynamic shift from direct glucose uptake to gluconate processing. These figures are in

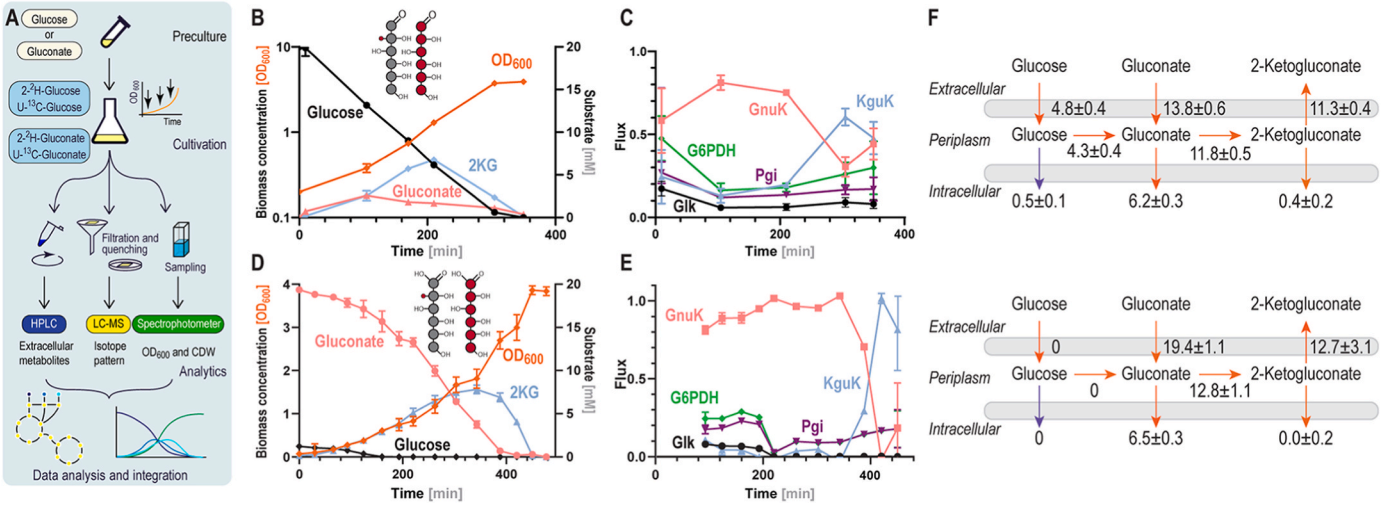

Fig. 4. Time-resolved D-fluxomic analysis for *P. putida* KT2440 growing on glucose or gluconate. (A) Workflow for time-resolved D-fluxomics. Bacteria were cultivated in de Bont minimal medium supplemented with labeled (U–^{13}C and 2-^{2}H) glucose. Over the cultivation, samples were periodically taken to determine cell density (optical density at 600 nm, OD_{600}, and cell dry weight, CDW), concentration of carbohydrates in the supernatant (by HPLC) and the labeling pattern of key metabolites (by LC-MS). These data were then combined to identify metabolic routes active during glucose-dependent batch cultivations. **(B)** Biomass and carbohydrate concentration profiles in batch cultures of wild-type *P. putida* KT2440 grown on glucose. Cells were grown on a mixture of 25% unlabeled glucose, 25% [2-^{2}H]-glucose and 50% [U–^{13}C]-glucose (total carbohydrate concentration = 20 mM). **(C)** Fluxes in the upper metabolism of *P. putida* KT2440 over time in glucose cultures. All fluxes were normalized to the total carbon uptake (i.e. $q_S = 1$). Abbreviations: Glk, glucose kinase; GnuK, gluconokinase; Pgi, phosphoglucoisomerase; G6PDH, glucose-6-phosphate dehydrogenase; KguD, 2-ketogluconate-6-phosphate reductase. Data represent mean values ± standard deviation of three independent experiments. **(D)** Biomass and carbohydrate concentration profiles in batch cultures of wild-type *P. putida* KT2440 grown on gluconate. Cells were grown on a mixture of 50% [U–^{13}C]-gluconate and 50% [2-^{2}H]-gluconate (total carbohydrate concentration = 20 mM; note that ca. 1 mM residual glucose was present in the medium at the onset of the cultivation). **(E)** Fluxes in the upper metabolism of *P. putida* KT2440 over time in gluconate cultures. All fluxes were normalized to the total carbon uptake (i.e. $q_S = 1$); data represent mean values ± standard deviations of three experiments. **(F)** Sugar uptake and distribution of fluxes within the periplasmic glucose oxidation in *P. putida* KT2440. Fluxes are shown for the early growth phase (upper panel) and the late growth phase, after gluconate depletion (lower panel). Fluxes were calculated from the relative uptake rates and biomass yields on the different substrates. In this metabolic map, fluxes are given as mmol $g_{CDW}^{-1}\ h^{-1}$; the growth rate in the early growth phase was $\mu = 0.78 \pm 0.08\ h^{-1}$ and $\mu = 0.38 \pm 0.04\ h^{-1}$ in the late growth phase.

accordance with previous fluxomics studies, where the flux through Glk ranged from 10% to 33% of the total carbon uptake. Importantly, the observed flux variation over time (Fig. 4C) contradicts the prevailing hypothesis that gluconate and 2KG reach a *pseudo*-steady state in the bacterial periplasm. Hence, a gradual transition from pure glucose phosphorylation towards a mixed sugar uptake seems to occur during the early phase of cultivation. While the difference between the flux through Glk at the first to all other time points was statistically significant ($P < 0.05$, Student's *t*-test), there was no relevant difference between the later time points. It seems plausible that glucose uptake and processing through Glk remains constant over time (at an average flux of 7.3% ± 1.5%) once sufficient amounts of gluconate and 2KG have accumulated in the medium. Indeed, the Glk flux was maintained within this range even when the glucose concentration dropped below the limit of quantification (~0.1 mM) at 350 min (Fig. 4B and **C**)—most likely due to the high-affinity nature of glucose uptake in *P. putida*. Orthologues of the glucose import system in other *Pseudomonas* species exhibit K_M values in the low-μM range (e.g. *P. aeruginosa*, *P. chlororaphis* and *P. fluorescens*; Table S2 in the Supplementary Material), thus supporting this notion.

Gluconate processing through GnuK dominated the overall carbon uptake profile during most of the experiment—except for the very late stage of the cultivation, when the gluconate concentration fell below 1.12 ± 0.08 mM (Fig. 4B). The main carbon uptake regime, in the form of gluconate, is fully aligned with previous reports (Kohlstedt and Wittmann, 2019; Nikel et al., 2015, 2021), where early-exponential phase cultures (OD_{600} = 0.2–0.6) were used to determine fluxes at a single time point. However, our data indicates that a significant fraction of 2KG was also taken up while there was more than 1 mM gluconate still present in the culture medium. An early study reported a K_M value for GnuK of 0.12 mM (Coffee and Hu, 1972), while the K_M of the gluconate transport system has been determined to be ~0.5 mM (Vicente et al., 1975). These kinetic parameters determined *in vitro* help explaining our results, as the gluconate importer would not be operating at saturation, which is directly linked to the decreasing flux through this route over time. Uptake, phosphorylation and reduction of 2KG through the sequential action of KgnuT, KguK and KguD remained low (<20%) until the late fermentation phase. A significantly increased 2KG uptake (60% ± 5%) occurred only when the gluconate concentration had dropped below a threshold concentration while 2KG was still present at relatively high amounts (at $t = 305$ min). Furthermore, when all available carbon substrates (i.e. glucose, gluconate and 2KG) were nearly depleted (at $t =$ 350 min), the magnitude of the fluxes through GnuK and KguK was in a similar range (44% ± 9% and 48% ± 9%, respectively; Fig. 4C). A reduction in the specific growth rate was observed at this phase—probably due to the fact that the overall carbon uptake rate was insufficient to support unlimited bacterial growth.

While the fluxes through the convergent uptake pathways displayed high plasticity during the whole batch cultivation, the fluxes within the EDEMP cycle remained fairly stable over time—as represented by the Pgi flux (Fig. 4C). Indeed, the Pgi flux was significantly elevated (27% ± 7%) only at early time points ($t < 20$ min), whereas no major differences were detected between the samples taken at later time points (12%–17%). G6PDH followed a similar trend as described for the Pgi activity: a high flux was detected at the first time point (48% ± 13%), with a relatively stable value during late cultivation (16%–30%). The highest Pgi and G6PDH fluxes in the first experimental measurements may be directly connected to the larger flux through Glk. By the end of the cultivation, a significantly higher flux through KguK, the phosphorylation step prior to the activity of KguD, a strictly NADPH-dependent dehydrogenase (Nikel et al., 2015), was accompanied by a slight increase in the EDEMP cycle fluxes—as indicated for the G6PDH flux. This observation may underlie a compensatory phenomenon, as there are only a few NADPH-producing reactions in the central carbon metabolism of *P. putida*, i.e. G6PDH, 6PGDH, MaeB, ICTDH and GDH (Volke et al., 2022). Moreover, these results are in line with the general defense mechanism deployed when *P. putida* deals with oxidative stress (and the associated NADPH demand), i.e. activation of the oxidative branch in the PP pathway and increased activities through G6PDH, caused by higher flux through Glk and recycling through Pgi (Nikel et al., 2021).

3.3.3. High-definition, time-resolved flux analysis of gluconate metabolism in *P. putida* KT2440

The dynamic changes in substrate consumption motivated us to conduct experiments at an even higher level of resolution, as the transition from gluconate-to-2KG uptake in glucose cultures happened rapidly (Fig. 4C). To this end, we slightly changed the experimental setup by using a mixture of 50% [U–^{13}C]- and 50% [2-^{2}H]-gluconate as the carbon source instead of glucose. We reasoned that this strategy would allow for enhanced and faster 2KG accumulation, thus enabling a better resolution of carbon uptake dynamics at late stages of the cultivation. Since [2-^{2}H]-gluconate is not commercially available, we prepared this labeled carbon substrate in a biotransformation reaction with resting cells of *P. putida* Gln (Δ*glk* Δ*gtsABCD* Δ*gnuK* Δ*gntT* Δ*gad*) incubated in the presence of [2-^{2}H]-glucose. Under our experimental conditions, resting-cell biotransformation experiments typically proceeded with a >95% efficiency in glucose oxidation. Also, in previous experiments carried out as shaken-flask cultivations, the cultures were shortly interrupted (<1 min) for sample withdrawal. To increase the resolution and quality of our experimental data, a frequent sampling routine was implemented by carrying out *P. putida* cultivations in temperature-controlled, baffled vessels with aeration provided by continuous magnetic stirring. This mini-bioreactor setup facilitated frequent sampling without significantly altering the culture conditions, and preliminary experiments showed that the overall physiology of *P. putida* KT2440 (e.g. specific growth rate and final OD_{600} values) was not significantly modified under these culture conditions as compared with shaken-flask cultivations (data not shown).

The novel cultivation setup led to the formation of high amounts of 2KG by *P. putida* (Fig. 4D), with up to 7.8 ± 0.5 mM 2KG accumulated after 343 min. The cultivation started with 1.2 ± 0.2 mM [2-^{2}H]-glucose still remaining in the culture medium, which dropped under the detection limit after 180 min. Interestingly, the Glk flux remained at relatively constant levels (7.2% ± 0.7%) while glucose was still detected (0.028 ± 0.002 mM at 160 min, Fig. 4E), similarly to glucose-dependent growth (Fig. 4C). The fact that no significant differences were observed for this flux between glucose and gluconate cultures strongly supports our hypothesis that direct glucose uptake by *P. putida* is stably maintained at ~7% if the sugar as well as gluconate are both present in the medium. The frequent sampling made it possible to catch a decrease in the Glk flux as the glucose concentration transitioned from ~10 μM (i.e. similar to the K_M of the glucose uptake system) to 0 μM. Indeed, this flux decreased to zero upon glucose depletion and remained as such at all later time-points.

Gluconate processing dominated sugar uptake in this experiment (Fig. 4D), with GnuK flux at 81–89%. Upon complete glucose depletion, gluconate was exclusively taken up (99% ± 3.8%) until its concentration decreased to 0.7 mM. The uptake of 2KG *via* KguK was low (4%–10%) while glucose was present in the culture medium. Once glucose was depleted, the KguK flux was negligible (0.6%) as long as gluconate was available. When the gluconate concentration dropped to 0.7 mM, KguK rapidly superseded GnuK as the predominant sugar processing flux. This Glk-GnuK-KguK flux transition was a rather revealing result, as this highly hierarchical and sequential uptake of the different carbon forms had never been described to this level of temporal resolution. The prevailing view was that the relative activities of the GnuK and KguK kinases determine the ratio of gluconate-to-2KG utilization. Similar to the hierarchy determined for the sugar uptake fluxes, three distinct growth phases were evidenced in the quantitative physiology data, which corresponded to growth until glucose depletion, followed by gluconate consumption and finally 2KG-dependent growth (Fig. S2 in the Supplementary Material). Upon glucose consumption, the specific growth rate decreased from $\mu = 0.78 \pm 0.08\ h^{-1}$ to $0.38 \pm 0.04\ h^{-1}$

(Figs. S2A and S2B), while the gluconate consumption increased from 13.8 ± 0.6 mmol g_{CDW}^{-1} h^{-1} to 19.4 ± 1.1 mmol g_{CDW}^{-1} h^{-1} (Figs. S2C and S2D). This shift was similar to the change in the specific rate of glucose consumption observed in the previous growth phase at 4.8 ± 0.4 mmol g_{CDW}^{-1} h^{-1} (Fig. S2B). The formation of 2KG was very similar during both phases (11.3 ± 0.4 mmol g_{CDW}^{-1} h^{-1} and 12.7 ± 3.1 mmol g_{CDW}^{-1} h^{-1}, respectively). Hence, the total rate of carbon uptake in the early growth phase was 5.7 ± 0.8 mmol g_{CDW}^{-1} h^{-1} and 2.5 ± 0.5 mmol g_{CDW}^{-1} h^{-1} in the later phase. Interestingly, there was no flux through KguK at 343 min (Fig. 4E), when 2KG peaked at 7.8 mM with gluconate at less than half that concentration (3.8 mM, Fig. 4D).

Since the transition between the different carbon uptake regimes occurred swiftly, without the biphasic (diauxic) growth behavior typically associated to adaptive gene expression, we hypothesized that these changes could be associated to post-transcriptional regulation. As indicated above, the co-consumption of glucose and 2KG could be triggered by the complementary use of $NADP^+$ and NADPH in both pathways—G6PDH produces NAD(P)H, whereas KguD consumes NADPH. Regulation of enzyme activity by NADPH availability is a common occurrence in bacteria (Christodoulou et al., 2018; Volke et al., 2021) and likely to govern carbon uptake as well. Because gluconate metabolism is energetically favorable compared to that of 2KG (with an energy yield of ~5.5 ATP *versus* ~1 ATP until Pyr is formed, respectively; Fig. 2D), catabolite repression may also play a role in controlling the hierarchical consumption of these oxidized substrates.

The changes in the peripheral carbon uptake routes on gluconate cultures were echoed by the EDEMP cycle fluxes (Fig. 4E). While gluconate and glucose were co-consumed, the Pgi flux remained at an average of 19.9% ± 2.5%, similarly to the previous experiments on glucose. In contrast, the Pgi flux was only 9.3% ± 0.4% when gluconate served as the sole carbon source, and gradually increased to ~18% as 2KG uptake became predominant. Higher EDEMP cycling during substrate co-utilization may reflect insufficient flux capacity in the lower EMP pathway, from glyceraldehyde-3-phosphate to pyruvate—which in turn might be associated to efficient protein allocation (Basan et al., 2015). This general argument is supported by the fact that the lower EMP reactions are less favored from a thermodynamic point of view and have higher protein costs than the reactions of the EDEMP cycle (Flamholz et al., 2013).

By combining the MFA data obtained through D-fluxomics with quantitative physiology parameters, we could calculate the exchange fluxes between glucose, gluconate and 2KG in the PGS (Fig. 4F). The transition from Glk to GnuK-KguK–predominant regimes when *P. putida* KT2440 grows on glucose was clearly captured by the distribution of fluxes in the PGS—at a degree of resolution that had been out of the scope of ^{13}C-MFA so far. The next step was investigating how tightly coupled the oxidation of glucose and gluconate is to biomass formation, and we set to conduct further experiments to elucidate this potential correlation.

3.4. Growth rate-dependent accumulation of gluconate and 2-ketogluconate in P. putida

Several studies reported on the accumulation and secretion of gluconate and 2KG when *Pseudomonas* species and related bacterial species face iron, phosphate or magnesium starvation (Buch et al., 2008; Sasnow et al., 2016; Uroz et al., 2020). The general paradigm is that glucose oxidation routes are upregulated to help solubilizing nutrients. However, we consistently observed gluconate and 2KG accumulation by engineered *Pseudomonas* strains, e.g. C2 auxotrophs (Wirth et al., 2022) and anthranilate producers (Fernández-Cabezón et al., 2022), under nutrient-sufficient growth conditions. A feature common to all these setups, however, is that bacterial growth was reduced as the concentration of oxidized sugars increased. On this background, we questioned whether the trigger for organic acids accumulation by *P. putida* could be a reduction in the growth rate rather than a specific starvation stimulus. This hypothesis was further impelled by our observation that resting (i.e. non-growing) cells of *P. putida* rapidly oxidized glucose to gluconate. Decoupling glucose oxidation from growth could be connected, among other factors, to the need of dissipating the energy acquired in the oxidation steps if not otherwise used, e.g. by H^+ leakage across the membrane (Nikaido, 2003), spontaneous ATP dephosphorylation (Meyrat and von Ballmoos, 2019) or water-forming NAD(P)H oxidation (Spaans et al., 2015). Therefore, a general mechanism was considered whereby carbon uptake is coupled to bacterial growth (i.e. at constant biomass yield), whereas the PGS activities are independent of growth. In this scenario, the accumulation of acids due to low growth rates would be merely an intrinsic characteristic of the system rather than a consequence of differential genetic or metabolic regulation. To explore this possibility, we ran shaken-flask cultures of *P. putida* KT2440 on glucose where the growth rate was artificially lowered by supplementation of chloramphenicol, a bacteriostatic antibiotic, at levels below the minimal inhibitory concentration. Chloramphenicol inhibits protein synthesis (Fernández et al., 2012), thereby slowing down bacterial growth. We periodically monitored bacterial growth, glucose consumption and formation of organic acids in these cultures until the primary carbon substrate was totally depleted (Fig. 5A). In the absence of any antibiotic, the specific growth rate of *P. putida* KT2440 cultivated in de Bont minimal medium supplemented with 20 mM glucose was $\mu = 0.66 \pm 0.02$ h^{-1}—similar to our previous observations. When chloramphenicol at 5 and 10 μg mL^{-1} was added to the *P. putida* cultures, the growth rates were reduced to $\mu = 0.46 \pm 0.02$ h^{-1} and 0.38 ± 0.01 h^{-1}, respectively (Fig. 5A)—although the final OD_{600} was similar in all cultures. The glucose consumption profile was similarly protracted in the presence of chloramphenicol, with sugar depletion at 7–8 h regardless of the antibiotic concentration. Importantly, the cultures with reduced growth rates transiently accumulated the two oxidized forms of glucose at significantly higher concentrations than in control conditions, without antibiotic. Hence, these observations expose an inverse correlation of gluconate and 2KG synthesis and the growth rate of glucose-grown *P. putida*.

To further test our hypothesis in a formal framework, we developed an *in silico* model to simulate *P. putida* batch cultivations. In this model, the activity of the Gcd and Gad oxidases depends solely on the cell density, whereas the uptake of glucose, gluconate and 2KG is correlated with both the biomass concentration and the specific growth rate. The model was parameterized with values for specific enzyme activity, glucose uptake rate, biomass yield and K_M values of the different transport systems taken from the literature on *P. putida* and related species (Table S2 in the Supplementary Material). Simulating glucose-dependent, batchwise growth of *P. putida* KT2440 at $\mu = 0.66$ h^{-1} (as experimentally determined, Figs. 5A) and 0.28 h^{-1} (i.e. a 60% reduction) predicted a significantly higher accumulation of gluconate and 2KG under slow-growing conditions (Fig. 5B). Interestingly, the model predicted no substantial glucose oxidation above a threshold growth rate, as the rate of consumption for the two acids would be higher than their rate of formation. Although the simplified model presented here neglects differential gene expression and protein allocation, which certainly influence glucose catabolism, it could predict gluconate and 2KG accumulation during glucose-containing batch cultivations of *P. putida* with a high degree of accuracy. Our simulations support the notion that acids accumulation is solely driven by the interplay of growth-coupled and growth-uncoupled reaction rates in the PGS. Indeed, when the experimentally-determined peak concentrations of gluconate and 2KG were plotted against the growth rate of glucose-grown *P. putida* KT2440, an inverse correlation was evident (Fig. 5C). The *y*-axis intercept for the [2KG] *versus* μ plot (i.e. $\mu = 0$ h^{-1}) was 19.7 ± 1.8 mM—thus closely matching the initial glucose concentration. The *y*-axis intercept for the [gluconate] *versus* μ plot was 8.2 ± 0.8 mM. Hence, these results suggest that non-growing *P. putida* cells would transform all glucose into 2KG with a maximum transient gluconate concentration of ~8 mM. Conversely, the x-axis intercept (i.e. the μ value at which no organic acids are produced from glucose) was around $\mu = 1$ h^{-1} for both linear regressions (Fig. 5C), mirroring the results obtained in the simulations.

Based on these results, we propose a general mechanistic model for

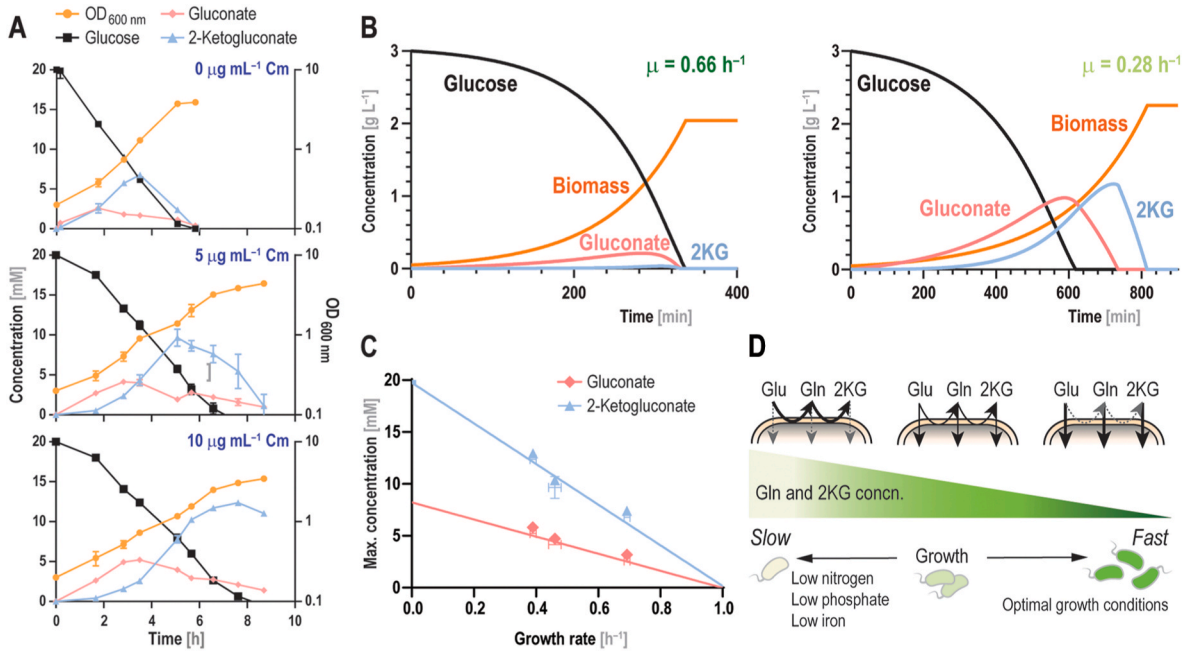

Fig. 5. Unveiling the mechanistic architecture of the periplasmic glucose shunt. (A) Growth profile and extracellular metabolite concentration for *P. putida* KT2440 grown on glucose in the presence of 0, 5 and 10 μg mL^{-1} chloramphenicol (Cm). Data represent mean values ± standard deviations of three independent experiments. **(B)** Modelling glucose consumption and gluconate and 2-ketogluconate (2KG) formation and uptake during batch cultivation of *P. putida* on glucose. Simulations were run with a growth rate μ = 0.66 h^{-1} (*left panel*) or with μ = 0.28 h^{-1} (*right panel*); other parameters used for *in silico* simulations are listed in Table S2 in the Supplementary Material. **(C)** Accumulation of gluconate and 2KG, expressed as the maximum (max.) concentration, in glucose-grown *P. putida* KT2440 as a function of the specific growth rate (μ). The initial glucose concentration was 20 mM; μ was artificially altered by Cm supplementation [see **(A)**]. The data point at μ = 0 h^{-1} for 2KG was calculated assuming 100% conversion; the slope for linear regressions for gluconate and 2KG concentration over time (t) are [gluconate] = $-8.24 \times t + 8.22$ ($R^2 = 0.96$) and [2KG] = $-19.57 \times t + 19.74$ ($R^2 = 0.98$), respectively. **(D)** Proposed mechanism for organic acid formation in slow-growing bacterial cultures. Assuming that the total carbon uptake is directly correlated to cell growth and that sugar oxidation is growth-independent, higher amounts of gluconate (Gln) and 2KG are secreted by slow-growing cells. Hence, oxidation of glucose (Glu) and gluconate is favored over carbon uptake during slow growth. Conversely, carbon uptake increases in fast-growing cells, while sugar oxidation remains unaffected.

the PGS activities in glucose-grown *P. putida* (Fig. 5D), whereby higher amounts of gluconate and 2KG are secreted by slow-growing cells. From a physiological perspective, sugar oxidation may seem wasteful at a first glance. Yet, this phenomenon likely arises as a trade-off between energy efficiency and tailoring environmental niches towards optimal growth—as secreted organic acids have solubilizing effects on some minerals (Brito et al., 2020; Phadungath and Metzger, 2011; Sashidhar and Podile, 2010). Furthermore, the PGS is relevant when glucose is highly abundant and not a growth-limiting nutrient—as reflected by the high K_M of Gcd = 4.91 mM (An and Moe, 2016). This metabolic scenario calls for great care in the analysis and interpretation of microbial physiology data, whenever the secretion of organic acids correlates with environmental stimuli that also influence the growth rate. Besides its relevance in Nature, the PGS is a key feature of *P. putida* amenable to engineering towards sugar-based biotechnological applications (Sánchez-Pascuala et al., 2019). In this case, the correlation between growth rate and acid production can be adopted as a proxy to predict fermentation parameters (Ankenbauer et al., 2020).

4. Conclusion and outlook

The PGS is a widespread metabolic motif in environmental bacteria that has eluded a quantitative, mechanistic explanation thus far. Early experimental evidence has shown that a major fraction of hexoses are not processed by direct phosphorylation but rather oxidized to gluconate and 2KG when *P. putida* is cultured in the presence of glucose (Vicente and Cánovas, 1973a, 1973b; Vicente et al., 1975). Moreover, a large part of the oxidized sugar pool is not taken up, but accumulated in the supernatant—becoming a substrate available for competitors in natural environments. What could be the advantage of bearing such a pathway for soil organisms?

Firstly, the total mineralization of glucose requires a considerable protein (enzyme) investment. As pointed out by Flamholz et al. (2013), there is a trade-off between enzymatic cost and energy gained from a given glycolytic pathway. This principle explains why the (energetically favorable) EMP pathway is not widespread, but many bacteria rely on the ED pathway instead (Chavarría et al., 2013). This occurrence is especially relevant in environmental microorganisms, e.g. the vast majority of marine bacteria (Klingner et al., 2015), cyanobacteria (Chen et al., 2016) and several non-model organisms (Fuhrer et al., 2005). The ED pathway plays also a crucial role in the human microbiome, as an *E. coli* strain deficient in this route cannot colonize the large intestine (Sweeney et al., 1996). The importance of gluconate for bacterial ecosystems is supported by its role as a signaling molecule for toxin production (Amirmozafari and Robertson, 1993). Secondly, and besides the biochemical reasons behind the coexistence of glucose processing pathways, competition between species is an important evolutionary driving force (Butaitė et al., 2017). Rather than adopting the absolute best biochemical strategy, bacteria have to outcompete other species in their environmental niches (Lugtenberg and Dekkers, 1999). The evidence presented here indicates that gluconate and 2KG secretion offers a competitive advantage that also helps understanding the widespread presence of the ED pathway. The PGS does neither require additional transporters nor initial phosphorylation of the carbon source, as do many other sugar processing pathways, and aerobic bacteria relying on the ED pathway could 'steal' sugar substrates from microbes utilizing solely the EMP—as they cannot consume gluconate or 2KG. Also, the enzymatic cost of the PGS is rather low (i.e. only two periplasmic oxidases, Gcd and Gad, are involved in the cognate reactions). Furthermore, each of the oxidase steps gains one H^+, a very efficient energy yield as

compared to other glycolytic routes, and, overall, the PGS is exergonic—but another glycolytic route has to be still employed as this oxidative sequence does not yield any precursors for biomass formation, besides ATP.

Developing and applying D-fluxomics determined all convergent fluxes in the PGS of *P. putida* KT2440. To the best of our knowledge, this is a first-case example on the use of D as a functional tracer for MFA towards resolving peripheral glucose oxidation pathways. Furthermore, time-course D-fluxomics revealed the highly dynamic nature of glucose metabolism in *P. putida*, where spatiotemporally segregated uptake of the different sugar forms highlighted a hierarchical glucose, gluconate and 2KG processing—an aspect that has been largely neglected in metabolic models of *Pseudomonas*. This is not a surprising occurrence, as the data gained form ^{13}C-MFA is usually provide as an average of substrate intake (Kohlstedt et al., 2010). The majority of data reported in the literature was obtained during mid-exponential growth (usually, at OD_{600} ~0.5) in batch cultures (Kohlstedt and Wittmann, 2019; Nikel et al., 2015, 2021). At this point, there is already considerable accumulation of gluconate and 2KG in the medium—therefore *P. putida* is exposed to a mixture of glucose and these metabolites, rather than growing exclusively on glucose as it does at the beginning of the cultivation.

With all of these considerations in mind, reporting the exact time point of sampling, together with the concentration of glucose and its oxidized derivatives, is of utterly importance to compare MFA results from different experimental setups. We note that this call for action is not a mere academic side-note, but it has important implications for metabolic engineering and bioprocess development. Indeed, our study demonstrates that the accumulation of gluconate and 2KG can be solely explained through a reduction in the growth rates, which could inform, for instance, feeding policies in fed-batch cultivations (Davis et al., 2015). Interestingly, the activity of the PGS in *P. putida* does not follow the same principles as the overflow metabolism typical of *E. coli* and yeast (i.e. the Crabtree effect)—where a reduction in the growth rate limits the formation of acetate or ethanol in a glucose-rich environment (Basan et al., 2015; Bernal et al., 2016; Shimizu and Matsuoka, 2019).

Finally, even when we focused on resolving the PGS fluxes, the analytical power of the D-fluxomics methodology could be upgraded if further fluxes are elucidated. Our D-fluxomics protocol can be easily combined with other methods and is fully compatible with the use of traditional isotopic tracers, e.g. [1–^{13}C]-glucose. Quantitative measurements of D-enrichment in downstream metabolites, e.g. intermediates from the tricarboxylic acid cycle and the PP pathway (Bujdoš et al., 2023), can be also included to increase resolution and coverage. In this sense, adopting D-based isotopic tracers enables either elucidation of fluxes that could not be resolved with ^{13}C-substrates or it improves analytical accuracy. These practical aspects are exemplified in our study, where the investigation of multiple isotopologues and isotopomers of F6P allowed for the resolution of fluxes within the PP pathway, the EDEMP cycle and the direct conversion of G6P to F6P *via* Pgi—as each of these pathways leads to a characteristic labeling pattern of F6P. While these developments will expand the scope of this methodology in the near future, we argue that D-fluxomics can be adopted as a powerful strategy for MFA of non-conventional microbial hosts.

Authors' contributions

D.C.V. · Conceptualization, Investigation, Data curation, Methodology, Validation, Visualization, Writing–original draft; **N.G.** · Investigation; **R.M.** · Investigation; **P.I.N.** · Conceptualization, Resources, Funding acquisition, Supervision, Project administration, Writing–review & editing.

Ethics statement

The work presented in this article follows all prevailing local, national and international regulations and conventions, and normal scientific ethical practices.

Declaration of competing interest

The authors declare no conflict of interest.

Data availability

Data will be made available on request.

Acknowledgments

The financial support from The Novo Nordisk Foundation (NNF10CC1016517 and NNF18CC0033664) and from the European Union's *Horizon2020* Research and Innovation Program under grant agreement No. 814418 (*SinFonia*) to **P.I.N.** is gratefully acknowledged. The responsibility of this article lies with the authors. The NNF and the European Union are not responsible for any use that may be made of the information contained therein.

Appendix A. Supplementary data

Supplementary data to this article can be found online at https://doi.org/10.1016/j.ymben.2023.07.004.

References

Allen, D.K., Young, J.D., 2020. Tracing metabolic flux through time and space with isotope labeling experiments. Curr. Opin. Biotechnol. 64, 92–100.

Amirmozafari, N., Robertson, D.C., 1993. Nutritional requirements for synthesis of heat-stable enterotoxin by *Yersinia enterocolitica*. Appl. Environ. Microbiol. 59, 3314–3320.

An, R., Moe, L.A., 2016. Regulation of pyrroloquinoline quinone-dependent glucose dehydrogenase activity in the model rhizosphere-dwelling bacterium *Pseudomonas putida* KT2440. Appl. Environ. Microbiol. 82, 4955–4964.

Ankenbauer, A., Schäfer, R.A., Viegas, S.C., Pobre, V., Voß, B., Arraiano, C.M., Takors, R., 2020. *Pseudomonas putida* KT2440 is naturally endowed to withstand industrial-scale stress conditions. Microb. Biotechnol. 13, 1145–1161.

Bachmann, H., Fischlechner, M., Rabbers, I., Barfa, N., Branco dos Santos, F., Molenaar, D., Teusink, B., 2013. Availability of public goods shapes the evolution of competing metabolic strategies. Proc. Natl. Acad. Sci. U.S.A. 110, 14302–14307.

Bagdasarian, M., Lurz, R., Rückert, B., Franklin, F.C.H., Bagdasarian, M.M., Frey, J., Timmis, K.N., 1981. Specific purpose plasmid cloning vectors. II. Broad host range, high copy number, RSF1010-derived vectors, and a host-vector system for gene cloning in *Pseudomonas*. Gene 16, 237–247.

Bar-Even, A., Flamholz, A., Noor, E., Milo, R., 2012. Rethinking glycolysis: on the biochemical logic of metabolic pathways. Nat. Chem. Biol. 8, 509–517.

Basan, M., Hui, S., Okano, H., Zhang, Z., Shen, Y., Williamson, J.R., Hwa, T., 2015. Overflow metabolism in *Escherichia coli* results from efficient proteome allocation. Nature 528, 99–104.

Bednarski, T.K., Rahim, M., Young, J.D., 2021. *In vivo* ^{2}H/^{13}C flux analysis in metabolism research. Curr. Opin. Biotechnol. 71, 1–8.

Belda, E., van Heck, R.G.A., López-Sánchez, M.J., Cruveiller, S., Barbe, V., Fraser, C., Klenk, H.P., Petersen, J., Morgat, A., Nikel, P.I., Vallenet, D., Rouy, Z., Sekowska, A., Martins dos Santos, V.A.P., de Lorenzo, V., Danchin, A., Médigue, C., 2016. The revisited genome of *Pseudomonas putida* KT2440 enlightens its value as a robust metabolic *chassis*. Environ. Microbiol. 18, 3403–3424.

Bernal, V., Castaño-Cerezo, S., Cánovas, M., 2016. Acetate metabolism regulation in *Escherichia coli*: carbon overflow, pathogenicity, and beyond. Appl. Microbiol. Biotechnol. 100, 8985–9001.

Bilbao, A., Munoz, N., Kim, J., Orton, D.J., Gao, Y., Poorey, K., Pomraning, K.R., Weitz, K., Burnet, M., Nicora, C.D., Wilton, R., Deng, S., Dai, Z., Oksen, E., Gee, A., Fasani, R.A., Tsalenko, A., Tanjore, D., Gardner, J., Smith, R.D., Michener, J.K., Gladden, J.M., Baker, E.S., Petzold, C.J., Kim, Y.M., Apffel, A., Magnuson, J.K., Burnum-Johnson, K.E., 2023. PeakDecoder enables machine learning-based metabolite annotation and accurate profiling in multidimensional mass spectrometry measurements. Nat. Commun. 14, 2461.

Bitzenhofer, N.L., Kruse, L., Thies, S., Wynands, B., Lechtenberg, T., Rönitz, J., Kozaeva, E., Wirth, N.T., Eberlein, C., Jaeger, K.E., Nikel, P.I., Heipieper, H.J., Wierckx, N., Loeschcke, A., 2021. Towards robust *Pseudomonas* cell factories to harbour novel biosynthetic pathways. Essays Biochem. 65, 319–336.

Brito, L.F., López, M.G., Straube, L., Passaglia, L.M.P., Wendisch, V.F., 2020. Inorganic phosphate solubilization by rhizosphere bacterium *Paenibacillus sonchi*: gene expression and physiological functions. Front. Microbiol. 11, 588605.

Buch, A., Archana, G., Naresh Kumar, G., 2008. Metabolic channeling of glucose towards gluconate in phosphate-solubilizing *Pseudomonas aeruginosa* P4 under phosphorus deficiency. Res. Microbiol. 159, 635–642.
Bujdoš, D., Popelářová, B., Volke, D.C., Nikel, P.I., Sonnenschein, N., Dvořák, P., 2023. Engineering of *Pseudomonas putida* for accelerated co-utilization of glucose and cellobiose yields aerobic overproduction of pyruvate explained by an upgraded metabolic model. Metab. Eng. 75, 29–46.
Butaitė, E., Baumgartner, M., Wyder, S., Kümmerli, R., 2017. Siderophore cheating and cheating resistance shape competition for iron in soil and freshwater *Pseudomonas* communities. Nat. Commun. 8, 414.
Calero, P., Nikel, P.I., 2019. Chasing bacterial *chassis* for metabolic engineering: a perspective review from classical to non-traditional microorganisms. Microb. Biotechnol. 12, 98–124.
Caspi, R., Billington, R., Fulcher, C.A., Keseler, I.M., Kothari, A., Krummenacker, M., Latendresse, M., Midford, P.E., Ong, Q., Ong, W.K., Paley, S., Subhraveti, P., Karp, P. D., 2018. The MetaCyc database of metabolic pathways and enzymes. Nucleic Acids Res. 46, D633–D639.
Chavarría, M., Nikel, P.I., Pérez-Pantoja, D., de Lorenzo, V., 2013. The Entner-Doudoroff pathway empowers *Pseudomonas putida* KT2440 with a high tolerance to oxidative stress. Environ. Microbiol. 15, 1772–1785.
Chen, X., Schreiber, K., Appel, J., Makowka, A., Fähnrich, B., Roettger, M., Hajirezaei, M. R., Sönnichsen, F.D., Schönheit, P., Martin, W.F., Gutekunst, K., 2016. The Entner-Doudoroff pathway is an overlooked glycolytic route in cyanobacteria and plants. Proc. Natl. Acad. Sci. U.S.A. 113, 5441–5446.
Christodoulou, D., Link, H., Fuhrer, T., Kochanowski, K., Gerosa, L., Sauer, U., 2018. Reserve flux capacity in the pentose phosphate pathway enables *Escherichia coli*'s rapid response to oxidative stress. Cell Syst 6, 569–578.
Coffee, C.J., Hu, A.S., 1972. The kinetic characterization of gluconokinase from a pseudomonad. Arch. Biochem. Biophys. 149, 549–559.
Davis, R., Duane, G., Kenny, S.T., Cerrone, F., Guzik, M.W., Babu, R.P., Casey, E., O'Connor, K.E., 2015. High cell density cultivation of *Pseudomonas putida* KT2440 using glucose without the need for oxygen enriched air supply. Biotechnol. Bioeng. 112, 725–733.
de Kok, S., Kozak, B.U., Pronk, J.T., van Maris, A.J.A., 2012. Energy coupling in *Saccharomyces cerevisiae*: selected opportunities for metabolic engineering. FEMS Yeast Res. 12, 387–397.
de Oliveira, R.D., Novello, V., da Silva, L.F., Gomez, J.G.C., Le Roux, G.A.C., 2021. Glucose metabolism in *Pseudomonas aeruginosa* is cyclic when producing polyhydroxyalkanoates and rhamnolipids. J. Biotechnol. 342, 54–63.
del Castillo, T., Ramos, J.L., Rodríguez-Herva, J.J., Fuhrer, T., Sauer, U., Duque, E., 2007. Convergent peripheral pathways catalyze initial glucose catabolism in *Pseudomonas putida*: genomic and flux analysis. J. Bacteriol. 189, 5142–5152.
Dolan, S.K., Kohlstedt, M., Trigg, S., Vallejo Ramírez, P., Kaminski, C.F., Wittmann, C., Welch, M., 2020. Contextual flexibility in *Pseudomonas aeruginosa* central carbon metabolism during growth in single carbon sources. mBio 11, 02684-19.
Dolan, S.K., Wijaya, A., Kohlstedt, M., Gläser, L., Brear, P., Silva-Rocha, R., Wittmann, C., Welch, M., 2022. Systems-wide dissection of organic acid assimilation in *Pseudomonas aeruginosa* reveals a novel path to underground metabolism. mBio 13, e02541-22.
Eisenberg, R.C., Dobrogosz, W.J., 1967. Gluconate metabolism in *Escherichia coli*. J. Bacteriol. 93, 941–949.
Escobar-Turriza, P., Hernández-Guerrero, R., Poot-Hernández, A.C., Rodríguez-Vázquez, K., Ramírez-Prado, J., Pérez-Rueda, E., 2019. Identification of functional signatures in the metabolism of the three cellular domains of life. PLoS One 14, e0217083.
Fan, J., Ye, J., Kamphorst, J.J., Shlomi, T., Thompson, C.B., Rabinowitz, J.D., 2014. Quantitative flux analysis reveals folate-dependent NADPH production. Nature 510, 298–302.
Fernández-Cabezón, L., Cros, A., Nikel, P.I., 2021. Spatiotemporal manipulation of the mismatch repair system of *Pseudomonas putida* accelerates phenotype emergence. ACS Synth. Biol. 10, 1214–1226.
Fernández-Cabezón, L., Rosich i Bosch, B., Kozaeva, E., Gurdo, N., Nikel, P.I., 2022. Dynamic flux regulation for high-titer anthranilate production by plasmid-free, conditionally-auxotrophic strains of *Pseudomonas putida*. Metab. Eng. 73, 11–25.
Fernández, M., Conde, S., de la Torre, J., Molina-Santiago, C., Ramos, J.L., Duque, E., 2012. Mechanisms of resistance to chloramphenicol in *Pseudomonas putida* KT2440. Antimicrob. Agents Chemother. 56, 1001–1009.
Flamholz, A., Noor, E., Bar-Even, A., Liebermeister, W., Milo, R., 2013. Glycolytic strategy as a tradeoff between energy yield and protein cost. Proc. Natl. Acad. Sci. U. S.A. 110, 10039–10044.
Fuhrer, T., Fischer, E., Sauer, U., 2005. Experimental identification and quantification of glucose metabolism in seven bacterial species. J. Bacteriol. 187, 1581–1590.
Hartmans, S., Smits, J.P., van der Werf, M.J., Volkering, F., de Bont, J.A., 1989. Metabolism of styrene oxide and 2-phenylethanol in the styrene-degrading *Xanthobacter* strain 124X. Appl. Environ. Microbiol. 55, 2850–2855.
Kanehisa, M., Furumichi, M., Sato, Y., Kawashima, M., Ishiguro-Watanabe, M., 2022. KEGG for taxonomy-based analysis of pathways and genomes. Nucleic Acids Res. 51, D587–D592.
Kelleher, J.K., 2001. Flux estimation using isotopic tracers: common ground for metabolic physiology and metabolic engineering. Metab. Eng. 3, 100–110.
Klingner, A., Bartsch, A., Dogs, M., Wagner-Döbler, I., Jahn, D., Simon, M., Brinkhoff, T., Becker, J., Wittmann, C., 2015. Large-scale ^{13}C flux profiling reveals conservation of the Entner-Doudoroff pathway as a glycolytic strategy among marine bacteria that use glucose. Appl. Environ. Microbiol. 81, 2408–2422.
Koebmann, B.J., Westerhoff, H.V., Snoep, J.L., Nilsson, D., Jensen, P.R., 2002. The glycolytic flux in *Escherichia coli* is controlled by the demand for ATP. J. Bacteriol. 184, 3909–3916.
Kohlstedt, M., Becker, J., Wittmann, C., 2010. Metabolic fluxes and beyond—systems biology understanding and engineering of microbial metabolism. Appl. Microbiol. Biotechnol. 88, 1065–1075.
Kohlstedt, M., Wittmann, C., 2019. GC-MS-based ^{13}C metabolic flux analysis resolves the parallel and cyclic glucose metabolism of *Pseudomonas putida* KT2440 and *Pseudomonas aeruginosa* PAO1. Metab. Eng. 54, 35–53.
Latrach-Tlemçani, L., Corroler, D., Barillier, D., Mosrati, R., 2008. Physiological states and energetic adaptation during growth of *Pseudomonas putida* mt-2 on glucose. Arch. Microbiol. 190, 141–150.
Lawson, C.E., Nuijten, G.H.L., de Graaf, R.M., Jacobson, T.B., Pabst, M., Stevenson, D.M., Jetten, M.S.M., Noguera, D.R., McMahon, K.D., Amador-Noguez, D., Lücker, S., 2021. Autotrophic and mixotrophic metabolism of an anammox bacterium revealed by *in vivo* ^{13}C and ^{2}H metabolic network mapping. ISME J. 15, 673–687.
Lehmann, W.D., 2017. A timeline of stable isotopes and mass spectrometry in the life sciences. Mass Spectrom. Rev. 36, 58–85.
Letunic, I., Bork, P., 2021. Interactive Tree of Life (*iTOL*) v5: an online tool for phylogenetic tree display and annotation. Nucleic Acids Res. 49, W293–W296.
Li, H., Yu, C., Wang, F., Chang, S.J., Yao, J., Blake, R.E., 2016. Probing the metabolic water contribution to intracellular water using oxygen isotope ratios of PO_4. Proc. Natl. Acad. Sci. U.S.A. 113, 5862–5867.
Low, J.C.M., Wright, A.J., Hesse, F., Cao, J., Brindle, K.M., 2023. Metabolic imaging with deuterium labeled substrates. Prog. Nucl. Magn. Reson. Spectrosc. 134–135, 39–51.
Lugtenberg, B.J., Dekkers, L.C., 1999. What makes *Pseudomonas* bacteria rhizosphere competent? Environ. Microbiol. 1, 9–13.
Matsushita, K., Fujii, Y., Ano, Y., Toyama, H., Shinjoh, M., Tomiyama, N., Miyazaki, T., Sugisawa, T., Hoshino, T., Adachi, O., 2003. 5-Keto-D-gluconate production is catalyzed by a quinoprotein glycerol dehydrogenase, major polyol dehydrogenase, in *Gluconobacter* species. Appl. Environ. Microbiol. 69, 1959–1966.
Mendler, K., Chen, H., Parks, D.H., Lobb, B., Hug, L.A., Doxey, A.C., 2019. AnnoTree: visualization and exploration of a functionally annotated microbial tree of life. Nucleic Acids Res. 47, 4442–4448.
Meyrat, A., von Ballmoos, C., 2019. ATP synthesis at physiological nucleotide concentrations. Sci. Rep. 9, 3070.
Niedenführ, S., Wiechert, W., Nöh, K., 2015. How to measure metabolic fluxes: a taxonomic guide for ^{13}C fluxomics. Curr. Opin. Biotechnol. 34, 82–90.
Nikaido, H., 2003. Molecular basis of bacterial outer membrane permeability revisited. Microbiol. Mol. Biol. Rev. 67, 593–656.
Nikel, P.I., Zhu, J., San, K.Y., Méndez, B.S., Bennett, G.N., 2009. Metabolic flux analysis of *Escherichia coli creB* and *arcA* mutants reveals shared control of carbon catabolism under microaerobic growth conditions. J. Bacteriol. 191, 5538–5548.
Nikel, P.I., Martínez-García, E., de Lorenzo, V., 2014. Biotechnological domestication of pseudomonads using synthetic biology. Nat. Rev. Microbiol. 12, 368–379.
Nikel, P.I., Chavarría, M., Fuhrer, T., Sauer, U., de Lorenzo, V., 2015. *Pseudomonas putida* KT2440 strain metabolizes glucose through a cycle formed by enzymes of the Entner-Doudoroff, Embden-Meyerhof-Parnas, and pentose phosphate pathways. J. Biol. Chem. 290, 25920–25932.
Nikel, P.I., Pérez-Pantoja, D., de Lorenzo, V., 2016. Pyridine nucleotide transhydrogenases enable redox balance of *Pseudomonas putida* during biodegradation of aromatic compounds. Environ. Microbiol. 18, 3565–3582.
Nikel, P.I., Fuhrer, T., Chavarría, M., Sánchez-Pascuala, A., Sauer, U., de Lorenzo, V., 2021. Reconfiguration of metabolic fluxes in *Pseudomonas putida* as a response to sub-lethal oxidative stress. ISME J. 15, 1751–1766.
Nogales, J., Mueller, J., Gudmundsson, S., Canalejo, F.J., Duque, E., Monk, J., Feist, A. M., Ramos, J.L., Niu, W., Palsson, B.Ø., 2020. High-quality genome-scale metabolic modelling of *Pseudomonas putida* highlights its broad metabolic capabilities. Environ. Microbiol. 22, 255–269.
Orth, J.D., Thiele, I., Palsson, B.Ø., 2010. What is flux balance analysis? Nat. Biotechnol. 28, 245–248.
Pedersen, B.H., Gurdo, N., Johansen, H.K., Molin, S., Nikel, P.I., La Rosa, R., 2021. High-throughput dilution-based growth method enables time-resolved exo-metabolomics of *Pseudomonas putida* and *Pseudomonas aeruginosa*. Microb. Biotechnol. 14, 2214–2226.
Pfeiffer, T., Schuster, S., Bonhoeffer, S., 2001. Cooperation and competition in the evolution of ATP-producing pathways. Science 292, 504–507.
Phadungath, C., Metzger, L.E., 2011. Effect of sodium gluconate on the solubility of calcium lactate. J. Dairy Sci. 94, 4843–4849.
Rabinowitz, J.D., Kimball, E., 2007. Acidic acetonitrile for cellular metabolome extraction from *Escherichia coli*. Anal. Chem. 79, 6167–6173.
Romano, A.H., Conway, T., 1996. Evolution of carbohydrate metabolic pathways. Res. Microbiol. 147, 448–455.
Russell, J.B., Cook, G.M., 1995. Energetics of bacterial growth: balance of anabolic and catabolic reactions. Microbiol. Rev. 59, 48–62.
Sambrook, J., Russell, D.W., 2001. Molecular cloning: a laboratory manual. In: Cold Spring Harbor Laboratory. Cold Spring Harbor.
Sánchez-Pascuala, A., Fernández-Cabezón, L., de Lorenzo, V., Nikel, P.I., 2019. Functional implementation of a linear glycolysis for sugar catabolism in *Pseudomonas putida*. Metab. Eng. 54, 200–211.
Sandberg, T.E., Long, C.P., Gonzalez, J.E., Feist, A.M., Antoniewicz, M.R., Palsson, B.Ø., 2016. Evolution of *E. coli* on [U-^{13}C]-glucose reveals a negligible isotopic influence on metabolism and physiology. PLoS One 11, e0151130.
Sashidhar, B., Podile, A.R., 2010. Mineral phosphate solubilization by rhizosphere bacteria and scope for manipulation of the direct oxidation pathway involving glucose dehydrogenase. J. Appl. Microbiol. 109, 1–12.

Sasnow, S.S., Wei, H., Aristilde, L., 2016. Bypasses in intracellular glucose metabolism in iron-limited *Pseudomonas putida*. Microbiol. 5, 3–20.
Schwechheimer, S.K., Becker, J., Wittmann, C., 2018. Towards better understanding of industrial cell factories: novel approaches for ^{13}C metabolic flux analysis in complex nutrient environments. Curr. Opin. Biotechnol. 54, 128–137.
Shimizu, K., Matsuoka, Y., 2019. Regulation of glycolytic flux and overflow metabolism depending on the source of energy generation for energy demand. Biotechnol. Adv. 37, 284–305.
Simon, J., van Spanning, R.J., Richardson, D.J., 2008. The organisation of proton motive and non-proton motive redox loops in prokaryotic respiratory systems. Biochim. Biophys. Acta 1777, 1480–1490.
Sone, N., Hägerhäll, C., Sakamoto, J., 2010. Aerobic respiration in the Gram-positive bacteria. In: Zannoni, D. (Ed.), Respiration in Archaea and Bacteria—Diversity of Prokaryotic Respiratory Systems, vol. 1. Springer, Dordrecht, The Netherlands, pp. 35–62.
Spaans, S.K., Weusthuis, R.A., van der Oost, J., Kengen, S.W., 2015. NADPH-generating systems in bacteria and archaea. Front. Microbiol. 6, 742.
Sweeney, N.J., Laux, D.C., Cohen, P.S., 1996. *Escherichia coli* F-18 and *E. coli* K-12 *eda* mutants do not colonize the streptomycin-treated mouse large intestine. Infect. Immun. 64, 3504–3511.
Torrontegui, D., Díaz, R., Cánovas, J.L., 1976. The uptake of 2-ketogluconate by *Pseudomonas putida*. Arch. Microbiol. 110, 43–48.
Unden, G., Bongaerts, J., 1997. Alternative respiratory pathways of *Escherichia coli*: energetics and transcriptional regulation in response to electron acceptors. Biochim. Biophys. Acta 1320, 217–234.
Uroz, S., Picard, L., Turpault, M.P., Auer, L., Armengaud, J., Oger, P., 2020. Dual transcriptomics and proteomics analyses of the early stage of interaction between *Caballeronia mineralivorans* PML1(12) and mineral. Environ. Microbiol. 22, 3838–3862.
Vicente, M., Cánovas, J.L., 1973a. Regulation of the glucolytic enzymes in *Pseudomonas putida*. Arch. Microbiol. 93, 53–64.
Vicente, M., Cánovas, J.L., 1973b. Glucolysis in *Pseudomonas putida*: physiological role of alternative routes from the analysis of defective mutants. J. Bacteriol. 116, 908–914.
Vicente, M., de Pedro, M.A., de Torrontegui, G., Cánovas, J.L., 1975. The uptake of glucose and gluconate by *Pseudomonas putida*. Mol. Cell. Biochem. 7, 59–64.
Volke, D.C., Friis, L., Wirth, N.T., Turlin, J., Nikel, P.I., 2020. Synthetic control of plasmid replication enables target- and self-curing of vectors and expedites genome engineering of *Pseudomonas putida*. Metab. Eng. Commun. 10, e00126.
Volke, D.C., Olavarría, K., Nikel, P.I., 2021. Cofactor specificity of glucose-6-phosphate dehydrogenase isozymes in *Pseudomonas putida* reveals a general principle underlying glycolytic strategies in bacteria. mSystems 6, e00014-21.
Volke, D.C., Martino, R.A., Kozaeva, E., Smania, A.M., Nikel, P.I., 2022. Modular (de) construction of complex bacterial phenotypes by CRISPR/nCas9-assisted, multiplex cytidine base-editing. Nat. Commun. 13, 3026.
Wang, J., Yan, Y., 2018. Glycolysis and its metabolic engineering applications. In: Yan, Y. (Ed.), Engineering Microbial Metabolism for Chemical Synthesis: Reviews and Perspectives. World Scientific Publishing, Singapore, pp. 1–34.
Weimer, A., Kohlstedt, M., Volke, D.C., Nikel, P.I., Wittmann, C., 2020. Industrial biotechnology of *Pseudomonas putida*: advances and prospects. Appl. Microbiol. Biotechnol. 104, 7745–7766.
Wijker, R.S., Sessions, A.L., Fuhrer, T., Phan, M., 2019. ^{2}H/^{1}H variation in microbial lipids is controlled by NADPH metabolism. Proc. Natl. Acad. Sci. U.S.A. 116, 12173–12182.
Wilkes, R.A., Mendonca, C.M., Aristilde, L., 2019. A cyclic metabolic network in *Pseudomonas protegens* Pf-5 prioritizes the Entner-Doudoroff pathway and exhibits substrate hierarchy during carbohydrate co-utilization. Appl. Environ. Microbiol. 85, e02084, 18.
Winsor, G.L., Griffiths, E.J., Lo, R., Dhillon, B.K., Shay, J.A., Brinkman, F.S., 2016. Enhanced annotations and features for comparing thousands of *Pseudomonas* genomes in the *Pseudomonas* genome database. Nucleic Acids Res. 44, D646–D653.
Wirth, N.T., Kozaeva, E., Nikel, P.I., 2020. Accelerated genome engineering of *Pseudomonas putida* by I-*Sce*I–mediated recombination and CRISPR-Cas9 counterselection. Microb. Biotechnol. 13, 233–249.
Wirth, N.T., Gurdo, N., Krink, N., Vidal-Verdú, A., Donati, S., Fernández-Cabezón, L., Wulff, T., Nikel, P.I., 2022. A synthetic C2 auxotroph of *Pseudomonas putida* for evolutionary engineering of alternative sugar catabolic routes. Metab. Eng. 74, 83–97.
Wirth, N.T., Funk, J., Donati, S., Nikel, P.I., 2023. *QurvE*: user-friendly software for the analysis of biological growth and fluorescence data. Nat. Protoc. https://doi.org/10.1038/s41596-41023-00850-41597 (in press).
Wishart, D.S., 2008. Quantitative metabolomics using NMR. Trends Anal. Chem. 27, 228–237.
Zamboni, N., Fendt, S.M., Rühl, M., Sauer, U., 2009. ^{13}C-based metabolic flux analysis. Nat. Protoc. 4, 878–892.
Zhu, W., Klinman, J.P., 2020. Biogenesis of the peptide-derived redox cofactor pyrroloquinoline quinone. Curr. Opin. Chem. Biol. 59, 93–103.
Zotter, A., Bäuerle, F., Dey, D., Kiss, V., Schreiber, G., 2017. Quantifying enzyme activity in living cells. J. Biol. Chem. 292, 15838–15848.